

POLITECNICO DI TORINO

Collegio di Ingegneria Civile

Corso di Laurea Magistrale in Ingegneria Civile



Tesi di Laurea Magistrale

Optimization of Hybrid Flat Slab at ULS

Relatori

Prof. Albert de la Fuente

Prof. Maurizio Taliano

Co-Relatore

PhD (c) Stanislav Aidarov

Studente

Luca Sutera

Luglio 2019

Summary

Summary of figures	4
Summary of tables.....	7
Abstract.....	8
1 Introduction.....	9
1.1 Scope	9
1.2 Methodology	10
2 State of the art	11
2.1 Fibre reinforced concrete	11
2.1.1 Fibres type	11
2.1.2 Steel fibres	13
2.2 Steel fibre reinforced concrete	14
2.3 Residual flexural tensile strength.....	18
2.4 Full-scale slab test	26
2.4.1 Full-scale slab test at Bissen (2004).....	26
2.4.2 Full-scale slab test at Tallin (2007).....	32
3 Design approach for ultimate limit state.....	35
3.1 Plastic Analysis	35
3.1.1 Upper and lower bound theorems	36
3.2 Yield Line Theory	37
3.2.1 Yield line analysis proceeds	38
3.3 Application of Yield-Line Method for Elevated Slabs.....	42
3.3.1 Mechanism I: global failure.....	42
3.3.2 Mechanism II: Local failure	46
3.4 Flexural strength of FRC element	48
3.5 The arrangement of steel reinforcement.....	50
3.5.1 Top reinforcement.....	50
3.5.2 Bottom reinforcement.....	51
3.6 Punching shear in SFRC.....	52
4 Parametric studies	56
4.1 Influence of f_{ck}	59
4.2 Influence of f_{R3k}	61
4.3 Influence of A_s^-/A_s^+	64
4.4 Redistribution of moments.....	67
5 Optimization of Hybrid Flat Slab.....	72
5.1 Static analysis.....	73

5.1.1	Verification at punching shear	77
5.2	Parametric studies	79
5.2.1	Influence of ultimate load.....	79
5.2.2	Influence of thickness of the flat slab.....	80
5.2.3	Influence of span number	81
5.2.4	Influence of f_{R3m}	82
5.3	Economic analysis.....	83
6	Conclusion	85
6.1	Future studies	85
	References.....	86
	Acknowledgements	87

Summary of figures

Figure 1: Cross sectional geometries of fibres [1]12

Figure 2 Different fibre geometries [2]12

Figure 3: Different types of steel fibres [2]14

Figure 4: Effects of fibre on the structural behaviour [3].....16

Figure 5: Steel fibre reinforced concrete cracking zones [3].....17

Figure 6: Fracture surface of steel fibre-reinforced concrete [3]17

Figure 7: Tensile behaviour of FRC in uniaxial stress state [3].....19

Figure 8: Typical tensile and flexural behavior of FRC [3]19

Figure 9: Typical arrangement for measuring CMOD [7].....20

Figure 10: RILEM test specimen20

Figure 11: Crack Mouth Opening Displacement [7].....21

Figure 12: An example of typical results from a bending test with a softening material behaviour. [6].....22

Figure 13: Tensile behavior of steel fibre reinforced concrete with different fibre content.....22

Figure 14: Simplified post-crack constitutive laws; plastic-rigid behavior and linear post cracking stress- crack opening. [6].....23

Figure 15: Layout of the test slab.....27

Figure 16: Construction of the full-scale HRFA slab test in Bissen, 2004 [9]28

Figure 17: Application of displacement transducers beneath the slab [9].....28

Figure 18: Uniformly distributed load on the HRFA full-scale forging test at Bissen, 2004.[9]29

Figure 19: Deflection under SLS in the central field [9].....30

Figure 20: (a) Loading frame position for corner field tests, (b) Photo of the yield lines cracking pattern of the corner field [9]31

Figure 21: Deformed slab after loading of an edge field [9]31

Figure 22: Figure (a) load-deflection curve center field (b) load-deflection curve edge field .32

Figure 23: Diagram of lines from the break to negative bending (a) and Diagram of lines from break to positive bending. (b). [9]32

Figure 24: Full scale test in Tallinn with test rig and deflection gauges to measure the deformation of the slab under the loads in the ult. [10]33

Figure 25: Point load vs. deformation in the full-scale HRFA forging test in Tallinn, 2007. [10]34

Figure 26: Moment vs curvature	36
Figure 27: Ductile moment-rotation diagram [16].....	38
Figure 28 Example of rules for Yield Line [11]	39
Figure 29 Example of collapse mechanism [12].....	40
Figure 30 Crack patterns in elevated concrete slabs with Mechanism I - II formed in: (a) x-direction; and (b) y-direction,[4].....	42
Figure 31 Yield line patterns for two most representative panels of E-SFRC slabs in: (a) x direction; and (b) y direction. [4]	43
Figure 32: Principle of virtual work to estimate the ultimate load-carrying capacity of interior panel of slab submitted to uniform distributed load, [4]	44
Figure 33: Principle of virtual work to determine ultimate load-carrying capacity of strip of interior panel of slab subjected to uniform distributed load and line load (parallel to yield lines).	45
Figure 34: Principle of virtual work to calculate flexural strength of elevated slab submitted to point load [4].....	46
Figure 35: Yield line patterns for local failure, [4]	47
Figure 36: Simplified stress/strain relationship including the residual flexural tensile strength of fibres [6]	48
Figure 37: Recommended values for β	54
Figure 38: Typical basic control perimeters around loaded areas.....	54
Figure 39: Proposed distribution of top of reinforcement [12].....	58
Figure 40: Cross section	59
Figure 41: $M_u - q_u$ vs f_{R3k}	60
Figure 42: q_u vs f_{R3k}	61
Figure 43: M_u vs f_{R3k}	61
Figure 44: Graph ultimate load q_u vs F_{R3k}	62
Figure 45: Graph ratio x/d vs f_{R3k}	63
Figure 46: Graph ratio M_{p-} / M_{p+} vs f_{R3k}	63
Figure 47: Graph ultimate load q_u vs Total steel reinforcement content[kg/m^3].....	65
Figure 48: Graph ultimate load x/d vs Total steel reinforcement content[kg/m^3]	66
Figure 49: Graph ultimate load $M_{p-} / M_{p+} [-]$ vs Total steel reinforcement content[kg/m^3]....	66
Figure 50: Simplified moment-curvature, $M-\chi$, diagram [16]	67
Figure 51: Evolution of deflection moment over the supports and central span sections in terms of load [16].....	68

Figure 52: Flat slab model deployed using Sap2000	69
Figure 53: Elastic Moment along the y direction obtained from SAP 2000	70
Figure 54: Percentual moment redistribution vs f_{R3k}	71
Figure 55: Total steel content vs. f_{R3k} , for a flat slab containing the Hybrid Reinforcement designed according to the proposed design method.	73
Figure 56: M-/M+ vs f_{R3k}	74
Figure 57: x/d vs f_{R3k}	74
Figure 58: Total steel content vs. f_{R3k} , for plastic and elastic analysis.....	76
Figure 59: Flat slab model deployed using Sap2000	77
Figure 60: Total steel content vs. f_{R3k} , for different ultimate loads	79
Figure 61: Total steel content vs. f_{R3k} , for different thickness of the slab.....	80
Figure 62: Total steel content vs. f_{R3k} , for different span number	81
Figure 63: Total steel content for characteristic and mean tensile strength of fibre	82
Figure 64. Oscillation costs [$\text{€}/\text{m}^3$].....	83

Summary of tables

Table 1: Physical properties of typical fibre [2].....	13
Table 2: Constitutive models in European codes and guidelines [8]	25
Table 3: Concrete mix components [9]	27
Table 4: Concrete mix components [10]	33
Table 5: Common concentrations of top reinforcement over columns when using Yield Line Design, where E.D= edge distance is the centerline of the column to the edge of slab and L is the length of the span. [12]	50
Table 6: Conventional reinforcing steel properties	57
Table 7: Concrete properties	57
Table 8: Fibre properties [15]	58
Table 9: Cases studied	60
Table 10: Cases studied	62
Table 11: Case studied.....	65
Table 12: Cases studied	69
Table 13: Flat slab proprieties.....	72
Table 14: Fibre proprieties.....	72
Table 15: Values of dead and live loads.....	73
Table 16: Results obtained for case analysed	75
Table 17: Verification at punching for $fR3k=0$	77
Table 18: Verification at punching for $fR3k=30$	78

Abstract

Nowadays, the use of steel fibre reinforced concrete (SFRC) is increased significantly in the field of construction industry. New standards and guidelines accepted this material as a structural one what, in turn, permitted to broad the area of SFRC application. Executed Steel Fibre Reinforced Concrete Slabs (ESFRCS) in the office building of LKS in Spain, Triangle office building in Estonia and Shopping Mall in Latvia could be the examples of the performed SFRC elements with high structural responsibility.

In fact, the implementation of SFRC for the execution of elevated slabs has the essential advantages in comparison with traditional solutions. Optimization of resources, reduction of execution time, decreasing of the environmental impact could be named, beyond a doubt, as ones of aforementioned advantages. However, it should be pointed out that steel bar reinforcement also provides clear benefits for the surface structural elements. The placement of rebars in the required areas due to a certain value of stresses is truly among of them (what is impossible in the case of fibres).

Therefore, within the thesis in question, the possibility of hybrid solution (rebars + steel fibres) for elevated slabs has been studied in detail. The Ultimate Limit State design of Hybrid Reinforced Concrete Elevated Slabs has been carried out in accordance with relevant guidelines. Changing the proportion of fibre and standard rebars content in the established structure, the parametric study has been developed in order to obtain the most suitable solution in terms of structural capacity and potential costs.

1 Introduction

During the last decades, the notable progress has been achieved in technology of concrete as a construction material. Nowadays, it could be found various approaches to enhance essential properties of concrete, such as durability, crack resistance, thermal characteristics, residual tensile strength, fire resistance and workability, for instance. One of the most innovative method to effect almost on all mentioned characteristics is, without any doubt, the presence of fibres in the concrete mix.

Initially, the application of fibre reinforced concrete (FRC) was limited due to the lack of experience and knowledge regarding this technological material. As a consequence, this type of concrete was used only for non-structural purposes or in the elements subjected to low tensile stresses, like FRC roads, industrial pavements and precast tunnel segments. However, the updated codes and guidelines expanded the area of FRC usage and it has been already executed a plenty of FRC elements with high structural responsibility and the performance of elevated steel fibre reinforced concrete slabs could be a clear example.

The execution of aforementioned pile supported slabs drew attention throughout the world due to the evident advantages which bring the implementation of fibres instead of traditional reinforcement such as optimization of the recourses, time savings and reduction of environmental impact. Also, the possibility of hybrid solutions (fibre + rebars) for the plane FRC structural elements has been recently analyzed.

1.1 Scope

Taking into consideration the relevance of the topic, the study in question has as its main purpose of optimizing the design of a slab at the ultimate limit state in terms of structural strength and cost with a fibre-reinforced concrete and conventional reinforcement, by assuming some initials design hypothesis.

1.2 Methodology

This thesis consists of five chapters and an introductory part. The introductory part gives a more comprehensive background to the subjects treated in the papers.

In Chapter 2, a literature study was done on fibre reinforced concrete to gain knowledge about the material and its behaviour, strength and properties. In this report, results from experimental tests found in literature, on slab with varying fibre contents, were used as reference values and their material data and properties were used as input data for the design calculations.

Chapter 3 of the thesis focuses on the theoretical bases and hypotheses taken into account for the structural calculation. The following topics are described: the principles and applications of yield line theory for the calculation of moments using the plastic theory, the constitutive law used for fibre-reinforced concrete, the assumptions concerning the positioning of the reinforcement bars and the contribution given by steel fibres to resistance to punching shear.

In chapter 4, it is carried out some parametric studies aimed to analyse the influence of the compressive and tensile strength of the fibre reinforced concrete on bending behaviour. The ratio between the negative and positive area of ordinary reinforcement is analyzed in order to verify if it affects the total amount of steel. At the end, it is studied the redistribution percentage of elastic moment for different cases.

In chapter 5, the optimization of hybrid reinforced concrete elevated slabs ultimate limit state design has been carried out in accordance with the guidelines. Changing the proportion of fibre and standard rebars content in the established structure, the parametric study has been developed in order to obtain the most suitable solution in terms of structural capacity. Finally, it is performed an analysis of potential costs.

The major conclusions are presented in chapter 6 with suggestions for future research.

2 State of the art

2.1 Fibre reinforced concrete

Plain concrete is a brittle material with high compressive strength in comparison with tensile one which is approximately ten times smaller. Therefore, the implementation of reinforcement is required in order to improve the tensile properties of the material. The traditional solution involves the placement of the steel reinforcing bars to increase the load carrying capacity in the zones subjected to considerable tensile and shear stresses.

Relatively new approach lies in the enhancement of concrete tensile strength by means of material modification which includes the addition of fibres to the concrete mix. The main purpose of the fibres is to bear the tensile stresses once the concrete element is cracked. Besides the tensile strength improvement, fibres could influence on other properties of concrete such as crack resistance, durability, fire resistance, fatigue resistance, ductility, etc. Also, it should be mentioned that the fibre could be added to the concrete mix for structural and non-structural purposes.

Generally, we can classify as structural fibres, those which considerably increase the breaking energy of the concrete in comparison with the plain one (in this case, their contribution should be considered in the design of the FRC elements). Non-structural fibres, in turn, are not to be considered in the design procedure as they are aimed to effect on certain properties which were described above.

2.1.1 Fibres type

There are a number of different parameters that effect on the properties and behaviour of fibre reinforced concrete, such as mechanical properties of the implemented fibres and their geometrical shape, for instance. Each fibre type is designed for a specific purpose which could be the improvement of tensile strength, control of drying shrinkage or the improvement of fire resistance.

One of the most essential parameter for the fibre is its geometrical characteristics which vary crucially depending on the specific purpose: fibres could be several millimeters of length (microfibres) up to 80 mm (macro-fibres). The diameters also differ significantly, from a

fraction of a micrometer to 2 mm. Also, the shape of the fibre should be taken into consideration due to impressive diversity of this aspect: they can be straight, wave-shaped, bow-shaped, toothed, the surface intended, twisted or irregular, as illustrated in Figure 1. The cross-section of fibres can be different and can have a circular, square, rectangular, triangular, elliptical and irregular cross-section as it is presented in Figure 2. Besides, in order to improve the adherence with the concrete, the fibres can present the shaped ends, undulations, corrugations, crushing, hooks, etc. [1][2]

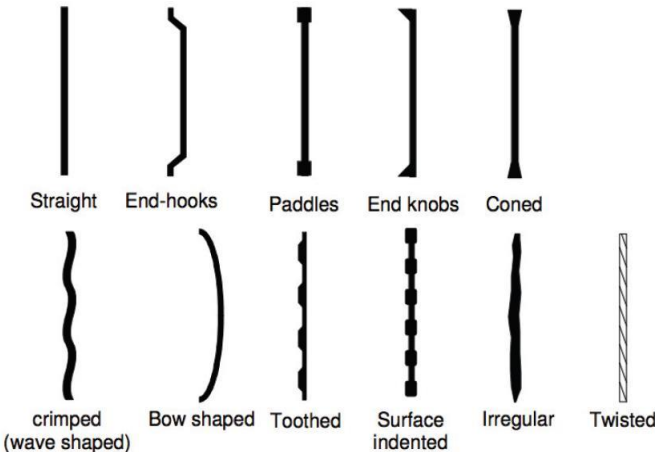


Figure 1: Cross sectional geometries of fibres [1]

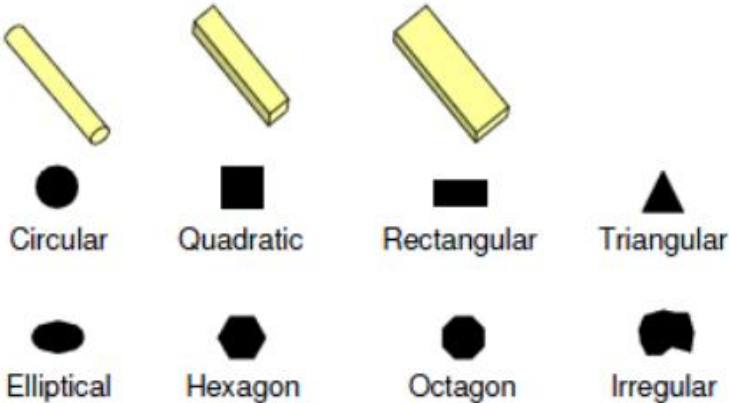


Figure 2 Different fibre geometries [2]

The mechanical properties of the fibres and their variety in dependence on the material could be noted in the Table 1.

Type of Fibre	Diameter [μm]	Specific gravity [g/cm^3]	Tensile strength [MPa]	Elastic modulus [GPa]	Ultimate elongation [%]
Metallic					
Steel	5-1 000	7.85	200-2 600	195-210	0.5-5
Glass					
E glass	8-15	2.54	2 000-4 000	72	3.0-4.8
AR glass	8-20	2.70	1 500-3 700	80	2.5-3.6
Synthetic					
Acrylic (PAN)	5-17	1.18	200-1 000	14.6-19.6	7.5-50.0
Aramid (e.g. Kevlar)	10-12	1.4-1.5	2 000-3 500	62-130	2.0-4.6
Carbon (low modulus)	7-18	1.6-1.7	800-1 100	38-43	2.1-2.5
Carbon (high modulus)	7-18	1.7-1.9	1 500-4 000	200-800	1.3-1.8
Nylon (polyamide)	20-25	1.16	965	5.17	20.0
Polyester (e.g. PET)	10-8	1.34-1.39	280-1 200	10-18	10-50
Polyethylene (PE)	25-1 000	0.96	80-600	5.0	12-100
Polyethylene (HPPE)	-	0.97	4 100-3 000	80-150	2.9-4.1
Polypropylene (PP)	10-200	0.90-0.91	310-760	3.5-4.9	6-15.0
Polyvinyl acetate (PVA)	3-8	1.2-2.5	800-3 600	20-80	4-12
Natural - organic					
Cellulose (wood)	15-125	1.50	300-2 000	10-50	20
Coconut	100-400	1.12-1.15	120-200	19-25	10-25
Bamboo	50-400	1.50	350-50	33-40	-
Jute	100-200	1.02-1.04	250-350	25-32	1.5-1.9
Natural - inorganic					
Asbestos	0.02-25	2.55	200-1 800	164	2-3
Wollastonite	25-40	2.87-3.09	2 700-4 100	303-530	-

Table 1: Physical properties of typical fibre [2]

From the presented in Table 1 types of fibres, steel ones are used the most in structural purposes. Given that this thesis focuses on elevated slabs which, by default, faces the considerable stresses, the above mentioned type of fibres is to be described in more detail.

2.1.2 Steel fibres

The steel fibres for concrete mix are discontinuous, with a discrete and uniform distribution that gives the material a high degree of homogeneity and isotropy. Generally, the dimensions of the steel fibres vary between 0.25 mm and 0.80 mm in diameter and the length is in the range from 10 up to 75 mm.

The following parameters are used in the characterization of steel fibres:

- Slenderness or aspect ratio: it is defined as the relationship between the length of the fibre and its diameter $\left(\frac{l_f}{\phi_f}\right)$.

- The tensile strength: this parameter depends on the quality of the steel. For a low or medium carbon content, the average resistance oscillates between 400 and 1500MPa, while it could reach 2000Mpa with higher carbon content.
- Shape: It has great importance for the adherence between fibre and concrete, as shown in chapter 2.1.1. It could be appreciated the variety of possible shapes in more detail by means of .



Figure 3: Different types of steel fibres [2]

The fibre length is recommended to be at least 2 times the size of the larger aggregate. Therefore, the length of steel fibres is usually of 2.5 to 3 times of the maximum aggregate size. In addition, the diameter of the pumping pipe requires that the length of the fibre be less than $\frac{2}{3}$ of the diameter of the pipe. However, the length of the fibre must be sufficient to give the necessary adhesion to the matrix and to avoid pull-outs too easily.

2.2 Steel fibre reinforced concrete

Steel fibre reinforced concrete (SFRC) is widely used in different fields of construction industry. The properties of steel fibres allows to improve both structural and non-structural characteristics of the material. However, it could be noted that recent studies are focused more on the possible applications of SFRC in structural purposes due to improved characteristics of the fibres (both mechanical and geometrical) and the appearance on new codes and guidelines as it was stated previously. Nowadays, the presence of fibres in the concrete mix is able to provide the partial or even total substitution of the conventional reinforcement due to high residual tensile strength, ductility and toughness of the material in question.

Experimental studies have shown that that normally used fibre volume in concrete does not lead to an increased strength before cracking. [3] The major role of the steel fibre reinforcement is to control the cracking of the concrete and give a contribution to the capacity after cracking.

The use of steel fibres is a well-acknowledged methodology to improve the tensile performance and toughness of concrete. Beside the better structural performances resulting from the enhanced mechanical properties, FRC allows a better shrinkage and crack control leading to increased structure durability. Stress redistribution resulting from the high internal redundancy of these structures may allow exploiting the post-cracking strength and toughness of SFRC, leading to a possible reduction of conventional reinforcement. The aforementioned partial or total substitution of conventional rebars allows reducing the construction time and costs in comparison with traditional Reinforced Concrete (RC) structures. [4]

Therefore, advantages of SFRC slab primarily include the economic aspects, followed by the improved strength and ductility, increased speed of construction, reduction of joints, and shrinkage crack width control in continuous joint-free slabs. Nevertheless, it should be noted that there is still some aspects to be covered and dynamic behavior, seismic design and long-term behavior are among them.

Mechanical properties

Steel fibres significantly increase the ductility of the concrete and also improve the residual tensile strength of the material. The main task of the added fibre is to bridge cracks that occur in the matrix and transfer tensile stresses across the cracks. The fibre contributes to improved crack control by causing large single cracks to be replaced by a system of microcracks with considerably smaller crack widths. [1]

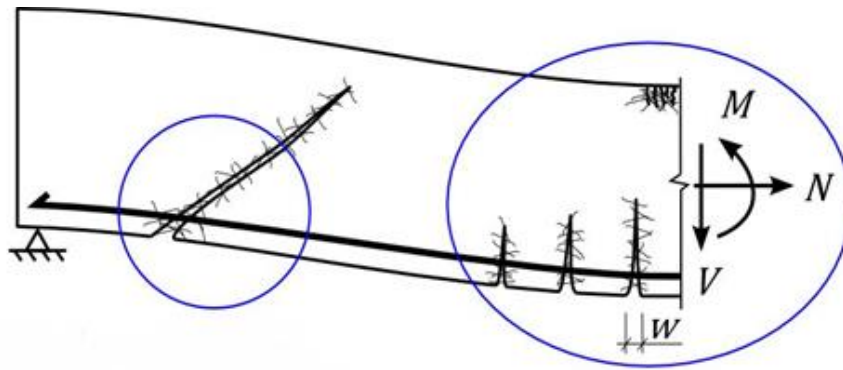


Figure 4: Effects of fibre on the structural behaviour [3]

Several studies and tests carried out over the years has highlighted some important properties, The effect of fibre in terms of crack bridging under the application of sectional forces M , V and N , Figure 4, are listed below. [1][4][5]

- Increased shear resistance
- Increased punching resistance
- Increased dowel effect
- Inhibits growth of splitting cracks
- Increased confinement of anchored bars
- Reduced crack spacing
- Reduced crack widths
- Increased moment resistance
- Increased flexural stiffness
- Increased ductility in compression

The post-cracking behavior of concrete, however, is significantly improved due to the fibre contribution. SFRC obtains a significant increase in the ultimate tensile strain and displays a distinct and stable residual tensile strength after cracking, even as the crack widths increase. [1]

Factors that influence on the material properties of fibre-reinforced concrete are the individual material properties of the matrix and the fibres, respectively, and the bond strength between the matrix and fibres. Furthermore, the amount of fibres, the orientation and distribution of fibres within the matrix are of importance.

The fibres is generally mixed into the concrete before pumping the concrete into the formwork, and the aim is to obtain a random fibres distribution and orientation. The distribution and the orientation of the fibres may be prevented from distributing freely and can be influenced by factors such as the method of placement, equipment used, such as reinforcement bars, and properties of the fresh concrete.

The fibre contribution leads to a more ductile failure for SFRC than for plain concrete, and the failure is mainly caused by fibre pull-out.[3] The tensile deformation capacity is improved, resulting in an increased critical crack opening. The critical crack opening is defined as the one where no stress can be transferred, as it is illustrated in Figure 5.

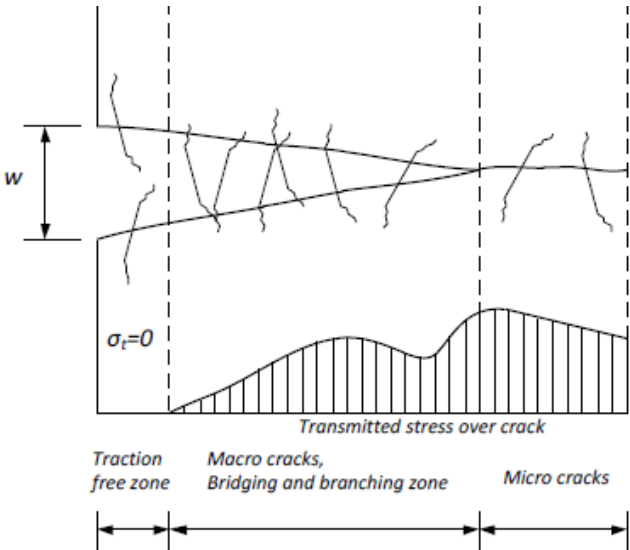


Figure 5: Steel fibre reinforced concrete cracking zones [3]

While Figure 6, shows a real fracture surface of SFRC after failure due to fibre pull-out, in which the randomly distributed and oriented fibres are clearly displayed.



Figure 6: Fracture surface of steel fibre-reinforced concrete [3]

Failure of SFRC due to fibre pull-out is desirable in order to obtain ductility and toughness during failure. Therefore, the fibre must be adequately ductile to prevent fibre fracture due to bending. Furthermore, the bond strength between the fibre and the matrix must be of the same magnitude, or higher, than the tensile strength of the matrix. [3]

For steel fibres with hooked ends a significant energy dissipation arises as the fibre is straightened and plastically deformed. This dissipated energy becomes part of the fracture energy of the concrete. The fracture energy is defined as the area under the stress-crack opening curve in tension and is the energy required for crack propagation [1]. Consequently, SFRC displays significantly higher fracture energy than plain concrete.

2.3 Residual flexural tensile strength

One of the most critical points in SFRC theory is to predict the tensile behavior of the material and especially to quantify the residual stresses in tension for a cracked section. After cracking, the SFRC displays a relatively stable residual tensile strength, even as the crack widths increase. The residual tensile strength, $f_{R,i}$, is defined as the residual tensile force resultant acting on a unit area of a cracked section in the concrete. During the design procedure, the contribution of fibres can be introduced by considering FRC as a homogeneous material with higher toughness, represented by the residual tensile strength.

Depending on the fibre content, the concrete might have strain-softening or hardening behaviour. A strain-softening material behavior is referred to as a behavior where the stress reduces with continuous development of plastic strains, whereas for strain-hardening material, the stress value increase after the crack deformation.

For deeper understanding of FRC behaviour, the uniaxial tension response of the material in question is showed in Figure 7. For strain-softening materials a localized single crack characterizes the tensile behavior, as seen in the tensile diagram.

Uniaxial tension

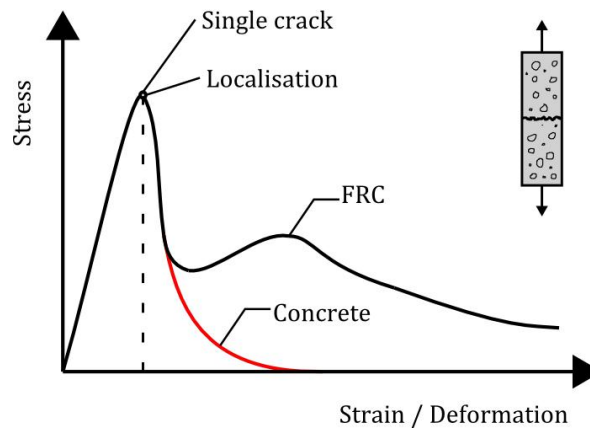


Figure 7: Tensile behaviour of FRC in uniaxial stress state [3]

In comparison to plain concrete, neither the tensile strength nor the modulus of elasticity of fibre-reinforced concrete is significantly affected. The fibre mainly affects the tensile fracture behavior and the post-cracking properties. For FRC with a low to moderate fibre content (< 1%) the stress-strain curve is characterized by a strain-softening behavior, as shown in figure 7. After the tensile strength is reached, the curve in this case decreases relatively steeply, but whereas the curve for plain concrete continues decreasing until zero. The curve for FRC typically increases again as the fibre starts acting by carrying tensile stresses across cracks. The last part of the curve, having an approximately constant stress value, displays the residual tensile strength of the FRC.

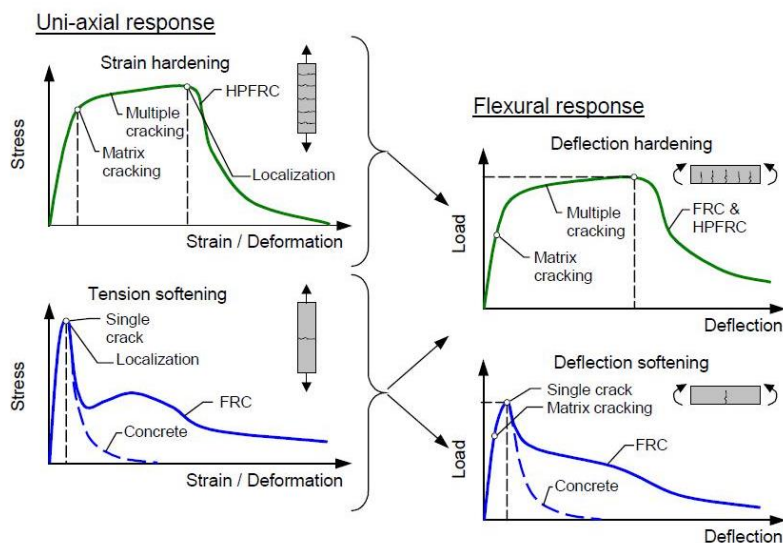


Figure 8: Typical tensile and flexural behavior of FRC [3]

Figure 8 shows typical tensile and flexural behavior of FRC. As it could be appreciated in the figure above that FRC can provide deflection hardening in bending despite the softening response in uni-axial tension. Also, it could be noted that in the case of softening behavior, the deformations localize in one crack, while the hardening one leads multiple cracking before reaching the peak value. [3]

Measuring the flexural tensile strength

According to FIB model code [6], the strength of fibres is measured as a residual flexural tensile strength. This can be done by performing three point bending test (3PBT). The main principle of the test is to evaluate the behaviour of SFRC in terms of residual flexural tensile strength values determined from the load-crack mouth displacement curve or load-deflection curve obtained by applying a centre-point load on a simply supported notched prism. The FIB model code proposes that it is to be done in accordance with EN 14651 (2005).[7]

The short description of the test procedure is: a simply supported beam with a span length of 500 mm and nominal size (width and depth) of 150 mm is to be tested. In the middle of the span, a notch is placed with a height of 25 mm and a maximum width of 5 mm, seen in Figure 9. A concentrated load is placed in the middle of the beam. The mentioned load should have the established rate of increase and at the same time the crack mouth opening displacement (CMOD) in the notch is to be measured. The result from the bending test of RILEM beam is shown in Figure 10 and 11

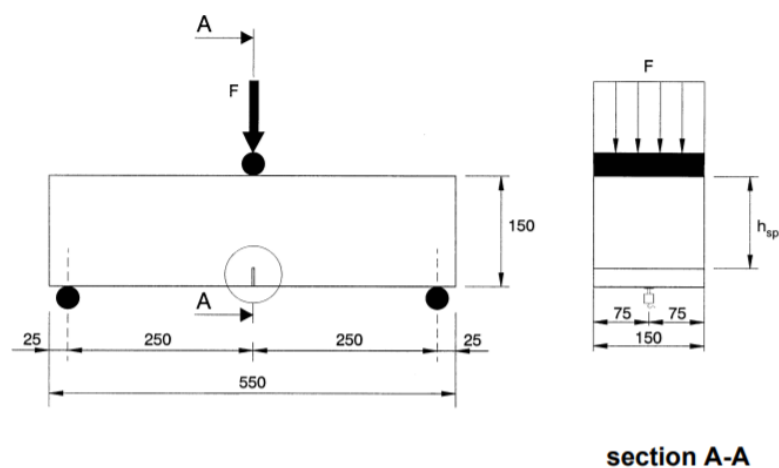


Figure 9: Typical arrangement for measuring CMOD [7]

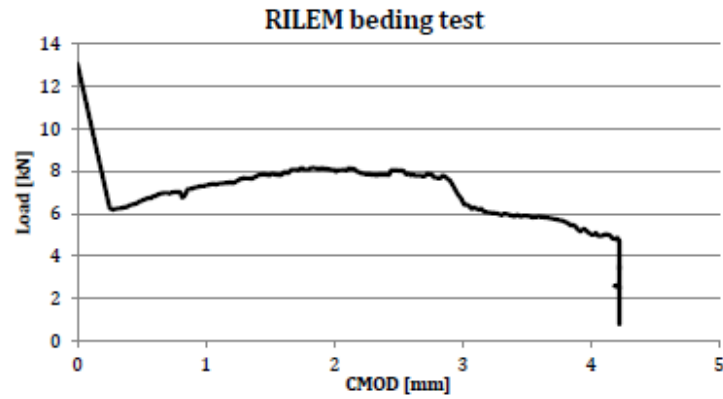


Figure 10: RILEM bending test [3]

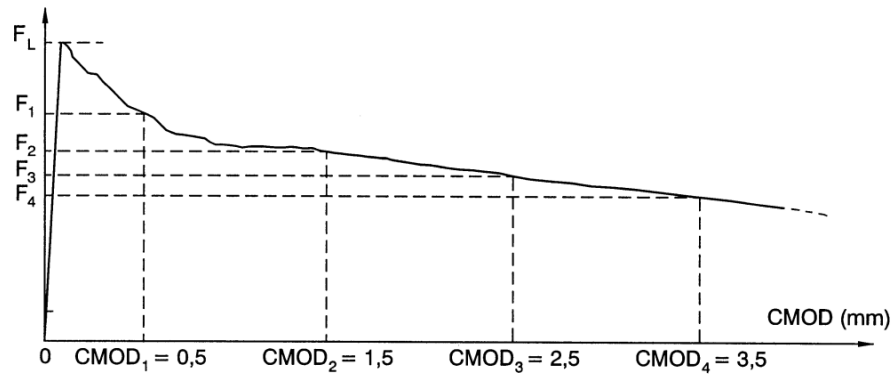


Figure 11: Crack Mouth Opening Displacement [7]

Different values of the residual flexural tensile strength, $f_{R,i}$, should be evaluated according to the following equation

$$f_{R,j} = \frac{3F_j l}{2bh_{sp}^2} \quad (2.1)$$

Where

$f_{R,i}$ is the residual flexural tensile strength corresponding to $CMOD_i$, [MPa]

F_i is the load corresponding to $CMOD_i$, [kN]

$CMOD_i$ is the crack mouth opening displacement, [mm]

l is the span of the specimen, [mm]

b is the width of the specimen, [mm]

h_{sp} is the distance between the notch tip and the top of the specimen, [mm]

The values f_{R1} and f_{R3} are obtained from the corresponding $CMOD_1$ and $CMOD_3$, respectively (Figure 12)

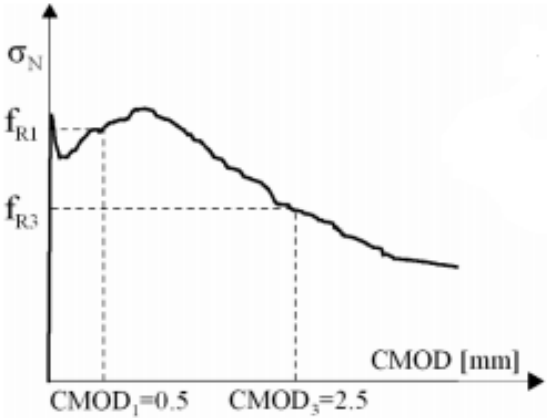


Figure 12: An example of typical results from a bending test with a softening material behaviour. [6]

The fibre content effects significantly on the residual tensile strength – CMOD curve as it possible to appreciate below:

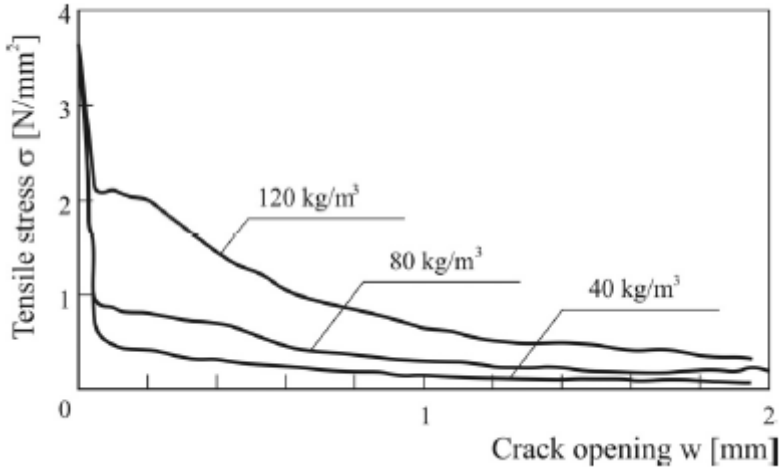


Figure 13: Tensile behavior of steel fibre reinforced concrete with different fibre content

Constitutive equation

The European standards and instructions which provide a constitutive equation of SFRC in tension are, in chronological order of appearance, the following:

- German standard DBV,
- RILEM,
- Italian standard CNR-DT 204,
- Spanish instruction EHE
- IB Model Code.

Most of them propose two diagrams, one for ultimate limit state design and the other one serviceability limit state. The proposed models could be obtained via different experimental tests for any SFRC mix. The three point bending test is the most common one for this objective. There are many constitutive models of the SFRC, both experimental and theoretical, and there is no one that imposes itself on the others. One of this is proposed from FIB Model Code.

The FIB model code simplifies the real response in tension, as shown in Figure 14, into two stress-crack opening constitutive laws, a linear post crack softening or hardening behavior, and a plastic rigid behavior,

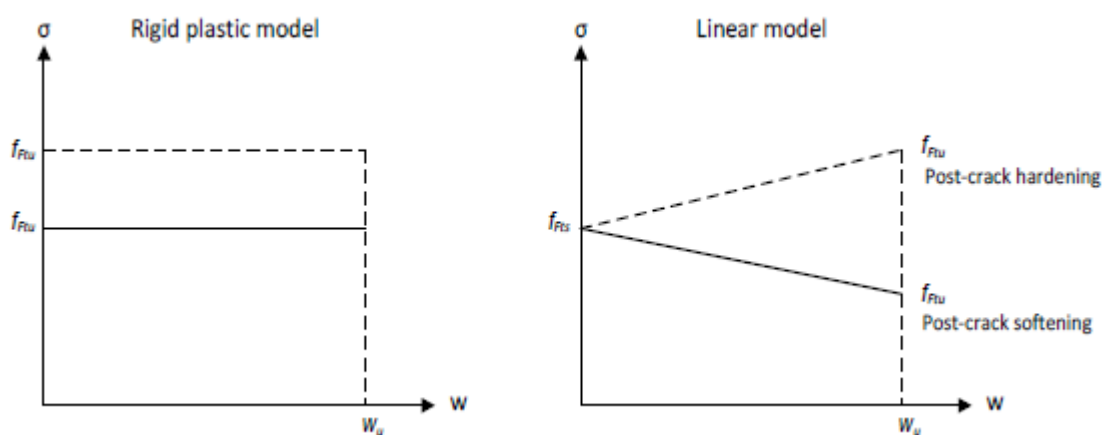


Figure 14 Simplified post-crack constitutive laws; plastic-rigid behavior and linear post cracking stress- crack opening. [6]

The parameter f_{Fts} represents the serviceability residual strength, defined as the post-cracking strength for crack opening at SLS. On the other hand, f_{Ftu} represents the ultimate residual strength and it is associated with the ULS crack opening w_u , which is the maximum crack opening accepted in the structural design and its value depends on the required ductility and therefore should not exceed 2.5mm, according to the FIB model code.

$$f_{Fts} = 0.45f_{R1} \quad (2.2)$$

$$f_{Ftu} = f_{Fts} - \frac{w_u}{CMOD_3} (f_{Fts} - 0.5f_{R3} + 0.2f_{R1}) \quad (2.3)$$

From a table produced by Ana Blanco [8] , it is possible to visualize the tensile behavior of the SFRC for the different standards. It should be mentioned that for the thesis in question, the rigid-plastic constitutive law has been applied in accordance with FIB Model Code.

Diagram	Parameters	Characterization test	
	$\sigma_1 = f_{eq,ctd,II} = f_{eq,ctk,II} \cdot \alpha_c^f \cdot \alpha_{sys} / \gamma_{ct}^f \leq f_{eq,ctd,I}$ (α_{sys} : coefficient for size effect; α_c^f : coefficient for long-term strength behaviour) $\epsilon_1 = \epsilon_u = 10\text{‰}$	DIN 1048 	DBV
	$\sigma_1 = f_{FTu} = f_{eq2}/3$ $\epsilon_1 = \epsilon_u = [20\text{‰ softening} ; 10\text{‰ hardening}]$	UNI 11039 	CNR-DT 204
	$\sigma_1 = f_{ctRd} = 0.33 f_{R3,d}$ $\epsilon_1 = \epsilon_u = [20\text{‰ bending} ; 10\text{‰ tensile}]$	UNE EN 14651 	EHE-08
	$\sigma_1 = f_{FTu} = f_{R3}/3$ $\epsilon_1 = \epsilon_u = [20\text{‰ softening} ; 10\text{‰ hardening}]$	UNE EN 14651 	MC2010
	$\sigma_1 = f_{eq,ctd,I} = f_{eq,ctk,I} \cdot \alpha_c^f \cdot \alpha_{sys} / \gamma_{ct}^f$ $\sigma_2 = f_{eq,ctd,II} = f_{eq,ctk,II} \cdot \alpha_c^f \cdot \alpha_{sys} / \gamma_{ct}^f \leq f_{eq,ctd,I}$ $\epsilon_2 = \epsilon_u = 10\text{‰}$	DIN 1048 	DBV
	$\sigma_1 = f_{FTS} = 0.45 f_{eq1}$ $\sigma_2 = f_{FTu} = k [f_{FTS} - (W_u/W_{I2}) (f_{FTS} - 0.5 f_{eq2} + 0.2 f_{eq1})]$ $k = [0.7 \text{ pure tension, } 1 \text{ other cases}]$ $\epsilon_2 = \epsilon_u = [20\text{‰ softening} ; 10\text{‰ hardening}]$	UNI 11039 	CNR-DT 204
	$\sigma_1 = f_{ctd} = \alpha_c^f \cdot f_{ctk,fl} / \gamma_{ct}$ $\sigma_2 = f_{eq,ctd,I} = f_{eq,ctk,I} \cdot \alpha_c^f \cdot \alpha_{sys} / \gamma_{ct}^f$ $\sigma_3 = f_{eq,ctd,II} = f_{eq,ctk,II} \cdot \alpha_c^f \cdot \alpha_{sys} / \gamma_{ct}^f \leq f_{eq,ctd,I}$ $\epsilon_1 = \sigma_1 / E_c ; \epsilon_2 = \epsilon_1 + 0.1\text{‰} ; \epsilon_3 = \epsilon_u = 10\text{‰}$	DIN 1048 	DBV
	$\sigma_1 = 0.7 f_{ctm,fl} (1.6 - d)$ $\sigma_2 = 0.45 \cdot K_h \cdot f_{R1}$ $\sigma_3 = 0.37 \cdot K_h \cdot f_{R4}$ $\epsilon_1 = \sigma_1 / E_c ; \epsilon_2 = \epsilon_1 + 0.1\text{‰} ; \epsilon_3 = \epsilon_u = 25\text{‰}$	RILEM TEST 	RILEM
	$\sigma_1 = f_{ct,d} = 0.6 f_{ct,fl,d}$ $\sigma_2 = f_{ctR1,d} = 0.45 f_{R1,d}$ $\sigma_3 = f_{ctR3,d} = k_1 (0.5 f_{R3,d} - 0.2 f_{R1,d})$ $\epsilon_2 = 0.1 + 1000 \cdot f_{ct,d} / E_c$ $\epsilon_3 = 2.5 / l_{cs}$ (l_{cs} : characteristic length) $\epsilon_u = [20\text{‰ bending} ; 10\text{‰ pure tension}]$	UNE EN 14651 	EHE-08
	$f_{ctm} = 0.30 (f_{ck})^{2/3}$ $f_{FTS} = 0.45 f_{R1}$ $f_{FTu} = k [f_{FTS} - (W_u / CMOD_3) (f_{FTS} - 0.5 f_{R3} + 0.2 f_{R1})]$ $\epsilon_{SLU} = W_u / l_{cs} = \min(\epsilon_{Fu}, 2.5 / l_{cs} = 2.5 / \gamma)$ $\epsilon_{Fu} = [20\text{‰ softening} ; 10\text{‰ hardening}]$	UNE EN 14651 	MC2010

Table 2: Constitutive models in European codes and guidelines [8]

2.4 Full-scale slab test

As it was stated previously, the high fibre content could totally substitute the traditional reinforcement in concrete structures. Despite the fact, that it is possible to verify the statement above by standard design approaches using the appropriate constitutive laws (see Subchapter 2.3), the experimental test were demanded due to the lack of experience in this area.

First full-scale tests to evaluate the structural behavior during the elastic and plastic phases of fibre-reinforced concrete were carried out in Bissen (2004) and Tallinn (2007). [9][10]

2.4.1 Full-scale slab test at Bissen (2004).

The slab was cast and tested in June 2004 and October 2004, respectively. The test consisted of determining the resistant capacity of a 200 mm thick slab with concrete reinforced with steel fibres. The main challenge of the experimental campaign in question was to execute the elevated steel fibre self-compacting concrete slab (ESFRSCCS) and to subject the latter to different types of load in order to evaluate the response of the structure. The full-scale specimen had the overall dimensions of 18,30 x 18,30 m and a designed thickness of 20 cm. As it is possible to appreciate in the Figure 15, the slab consisted of 9 fields and was supported by 16 steel columns with top plates of 30 x 30 cm. Keeping in mind the Canadian Standard, each column strip had an additional reinforcement in the lower surface to fulfil the requirement of anti-progressive collapse reinforcement.[9]

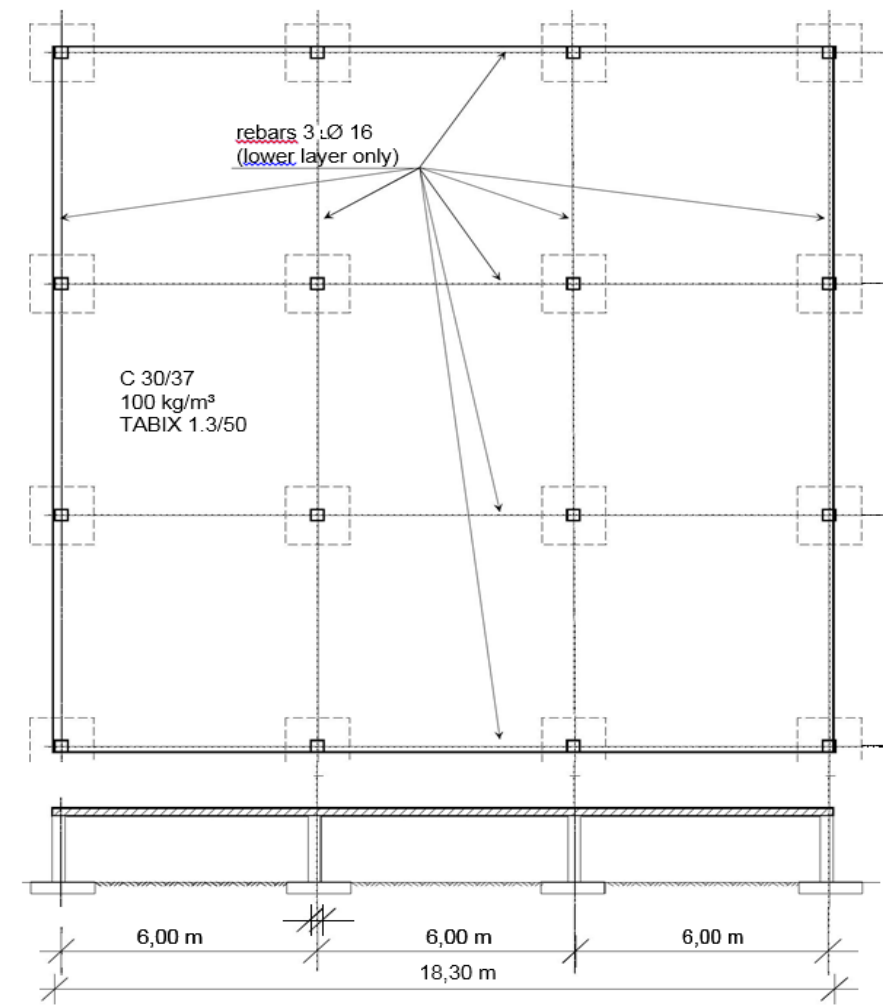


Figure 15: Layout of the test slab

In the following table 3, it is resumed the concrete mix components used in this test carried out.

Concrete mix components		
Designation	Unit	
Characteristic cylindrical compressive strength, f_{yk}	[MPa]	35
Cement content	[kg/m ³]	350
Water/cement	[-]	0,5
TABIX fibre dosage	[kg/m ³]	100
Steel fibres length	[mm]	50
Steel fibres diameter	[mm]	1,3
Steel tensile strength	[MPa]	900

Table 3: Concrete mix components [9]

It is possible to notice that the fibre content was impressive even though the appropriate workability was achieved as it possible to observe in the Figure 16



Figure 16: Construction of the full-scale HRFA slab test in Bissen, 2004 [9]

The SFRC was placed into the formwork, without any vibration, which results in a significant reduction in execution time and, therefore, a significant cost saving.

Before the application of loads, a precise leveling was performed by using an electronic leveling device. The leveling allows an accuracy of 0.1 mm. The slab was monitored from its lower face, as can be seen in Figure 17, using vertical strain gauges and strain gauges to detect the onset of cracks and the emergence of breaking lines.



Figure 17: Application of displacement transducers beneath the slab [9]

Initially, the flat slab was loaded with a uniformly distributed load of 1 to 6 kN/m² using tanks filled with water. (Figure 18).



Figure 18: Uniformly distributed load on the HRFA full-scale forging test at Bissen, 2004.[9]

All tanks were connected to each other by pipes. These connecting pipes allow equalization of the water level in each tank. The loads were gradually increased by filling the ballast tanks with water. Crack observations were carried out at load levels of $p = 1.00, 2.50, 3.00, 4.50$ and 6 kN/m^2 . The radial cracks on the top surface at the supports that already existed before life loads were applied did not increase significantly. On the lower surface, no cracks could be found. With this evenly distributed load, elastic deformations of less than 5 mm were obtained, which did not increase after seven days of placing the load. The load-deflection curves are shown in the Figure 19 and they show a linear elastic behavior. Initial cracks might occur in the real structure on top of the columns and probably in the field as well, but crack widths are much smaller than 0.2 mm.

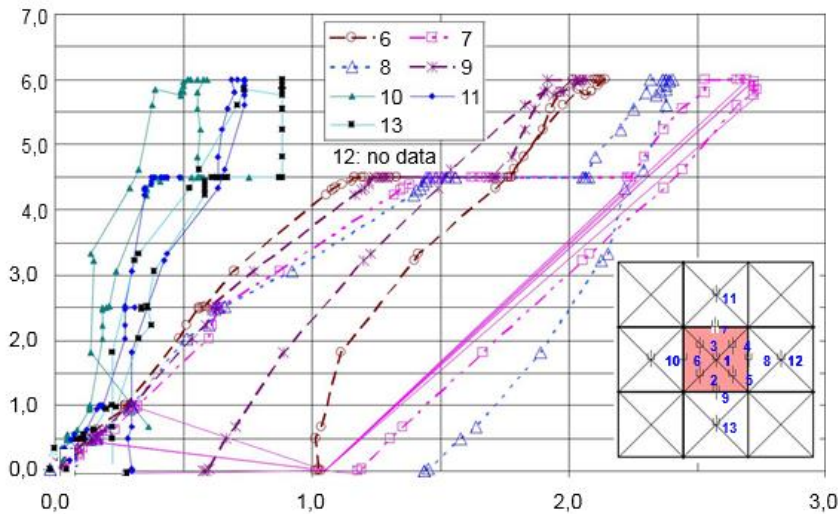
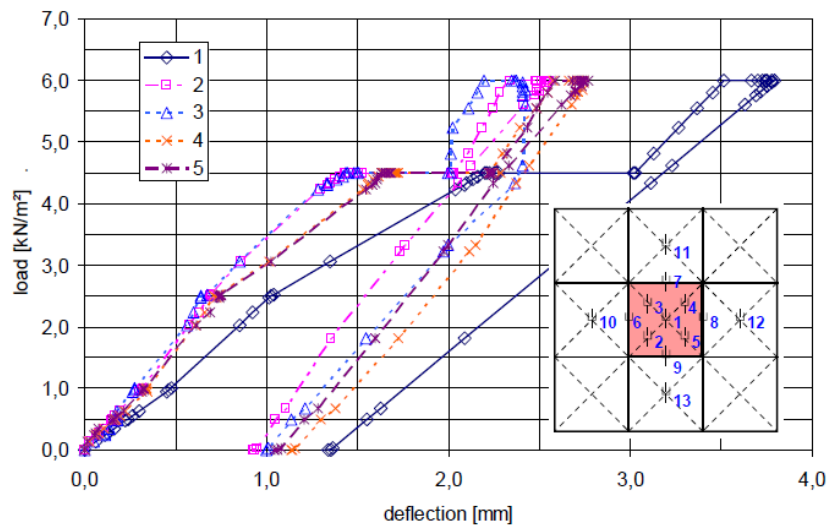


Figure 19: Deflection under SLS in the central field [9]

The last step of the testing program consisted of determining the ultimate load of the slab, by applying a central point load until breakdown. Obtained results proved the theoretically estimated behavior of the SFRC.[9]

Figures 20.a and 20.b show, respectively, an image of the point load test on a corner grid and the negative yield lines cracking pattern on the upper face of the corner field.

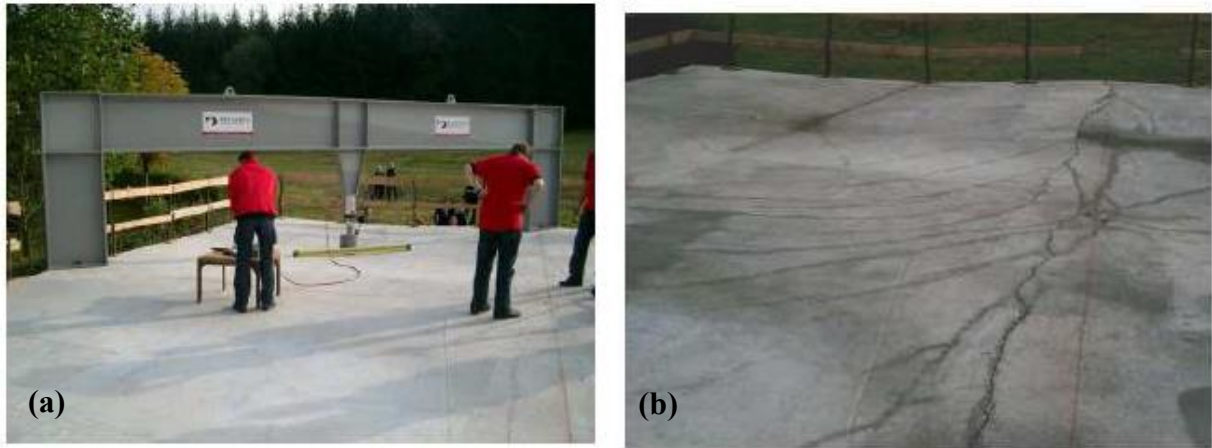


Figure 20: (a) Loading frame position for corner field tests, (b) Photo of the yield lines cracking pattern of the corner field [9]

Also, is possible to show the deformation of the edge slab under an acting load. (Figure 21).



Figure 21: Deformed slab after loading of an edge field [9]

In the central field a breaking load of 450 kN was reached, and in the corner areas a breaking load of 250 kN was reached. However, after reaching this last load, the plate still resisted a uniformly distributed constant load of 6 kN/m² up to a deformation of 260 mm without collapsing.

The final tests of the load bearing capacity of center, edge and corner fields were done by using a 700 kN hydraulic test cylinder with 200 mm stroke. The maximum load bearing capacity of the center field was $P_{\max} = 462.3$ kN. This was equal to a uniformly distributed load of $p = 25.7$ kN/m², including the self-weight of the structure the load bearing capacity was 30.7 kN/m², if the center field is loaded only.

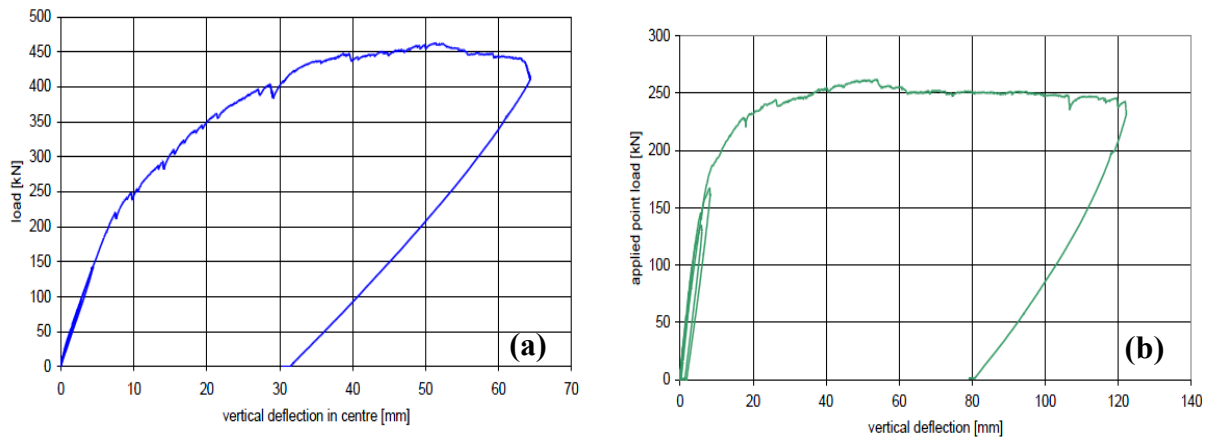


Figure 22: Figure (a) load-deflection curve center field (b) load-deflection curve edge field

The tested center, edge, and corner fields of the slab had developed a fan pattern of radial yield lines on the lower surface and tangential yield lines on the upper surface like shown in the Figure 23. Multiple cracking guaranteed small crack width even at loading conditions far above service loads. The slab had performed very ductile.

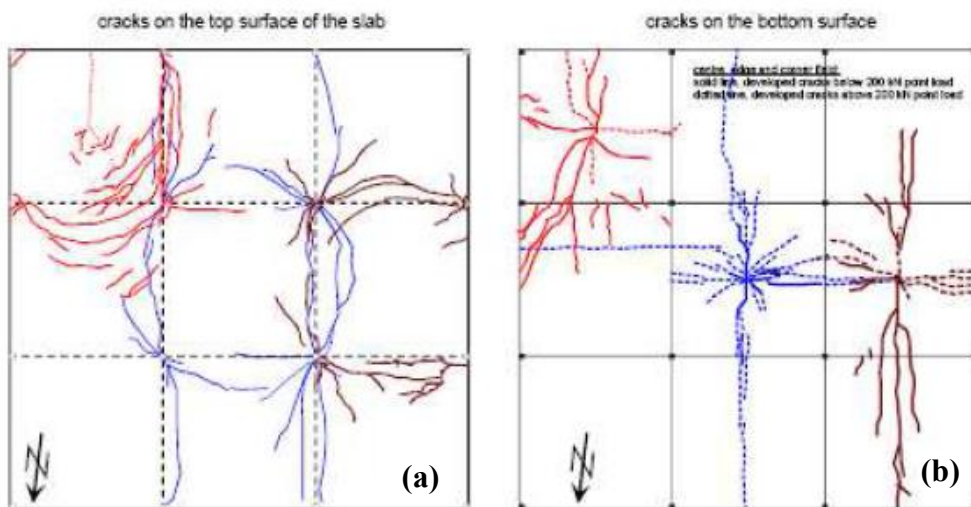


Figure 23: Diagram of lines from the break to negative bending (a) and Diagram of lines from break to positive bending. (b). [9]

2.4.2 Full-scale slab test at Tallin (2007).

Similarly to the Bissen experiment, the test carried out in Tallinn consisted of determining the strength of the 180 mm thick slab with steel fibre reinforced concrete, without passive reinforcement. The 5 meters span flat slab was executed and it was supported by 300x300 mm

square plan punctual supports, forming a regular arrangement of 4 x 4 of 16 pillars. [10]

Concrete mix components		
Designation	Unit	
Characteristic cylindrical compressive strength, f_{yk}	[MPa]	35
Cement content	[kg/m ³]	350
Water/cement	[-]	0,5
TABIX fibre dosage	[kg/m ³]	100
Steel fibres length	[mm]	50
Steel fibres diameter	[mm]	1,3
Steel tensile strength	[MPa]	900

Table 4: Concrete mix components [10]

As in the Bissen test, a uniformly distributed load of 6 kN/m² was applied, the effects of which were deformations of less than 5 mm. Concentrated loads were also imposed on the centre slab and also on the corner slab (Figure 24).

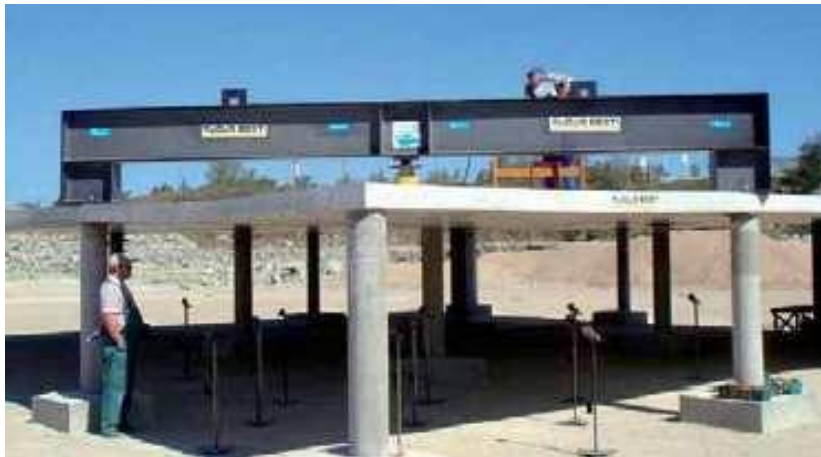


Figure 24: Full scale test in Tallinn with test rig and deflection gauges to measure the deformation of the slab under the loads in the uls. [10]

Figure 25 demonstrates the load-deformation curve obtained within the test. The point load was increased up to a value of 340 kN and then the prototype was unloaded. The last step of the experimental procedure was to lead the structure to a failure.

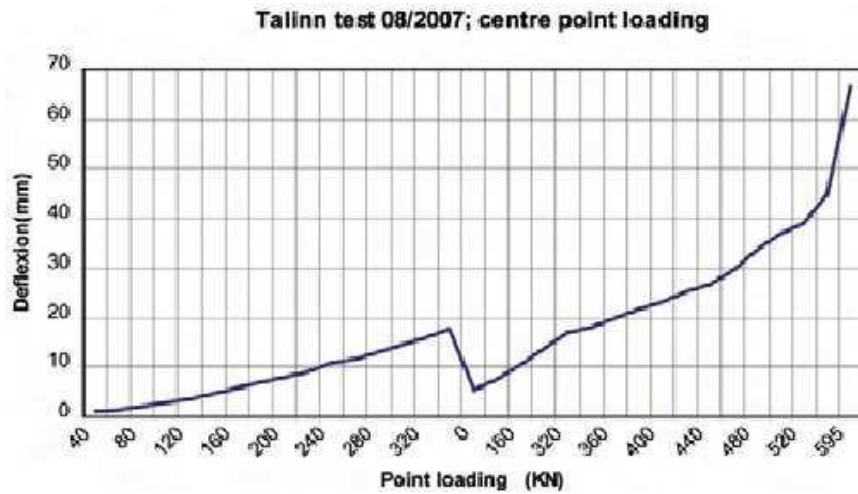


Figure 25: Point load vs. deformation in the full-scale HRFA forging test in Tallinn, 2007. [10]

The first crack appeared with a load of 125 kN and a vertical deformation under the load of 4 mm. The maximum load reached, as it is shown in the graph above, was 600 kN which led to an excessive cracking of the bottom surface of the slab. Load of 240 kN produced the deflection of 10 mm and it was reached just below the point of application of the point load without collapsing, what indicates an extremely ductile behavior of the SRFC slab, but with the formation of hundreds of cracks from 0.1 to 0.3 mm wide. From a load of 480 kN the cracks created increased their width to 3.5 mm.

Conclusion

Summarizing the obtained results of the described tests, it could be highlighted, that this new type of flat slab structures had proven its feasibility. As a brief conclusion, it could be noted the following:

- The design method involves both elastic analysis and plastic analysis to satisfy the serviceability limit state and ultimate limit state, respectively.
- There is a substantial increase in load from the appearance of the first crack to rupture due to the plasticity provided by the fibres and the high degree of hyperstaticism of the slab.
- To calculate the ultimate load is used the plastic theory, in this sense, the method of yield lines proposed by Johansen is compatible.

3 Design approach for ultimate limit state

ACI 544.6R-15 (American Concrete Institute) [4] provides the design procedure of the elevated concrete slabs which have steel fibres as the primary reinforcement. It should be noted, that still it is recommended to place a minimum amount of rebars, so called “anti-progressive collapse reinforcement”. [4] However, as it was demonstrated by several research studies, fibres represent a highly performing reinforcement for resisting diffused stresses, while localized stresses are better resisted by rebars. This means that one can use fibre reinforcement only, but the amount of fibres should be significantly increased in the whole structure in order to resist high stresses acting only in small areas. Therefore, new studies are focusing on combining fibres and rebars.

The design of SFRC structures is generally quite difficult as the non-linear tensile properties of the composite material have to be properly included in the calculations. Referring to SFRC slabs, the design procedures suggested by the codes are usually based on the Yield Lines Theory.

3.1 Plastic Analysis

The design procedure based on plastic analysis is only suitable when the critical sections have sufficient rotation capacity combined with possibility of the formation of plastic hinges, until the mechanism of structural collapse is obtained. Nevertheless, the fibres addition in the concrete matrix provides a high-ductile behavior, leading to a proper use of the plastic theory.

The plastic analysis should be based either on the lower bound (static) or the upper bound (kinematic) theorem, described in the chapter 3.1.1. When applying methods based on the theory of plasticity it should be ensured that the deformation capacity of critical areas is sufficient for the envisaged mechanism to be developed. The effects of previous applications of loading may generally be ignored and a monotonic increase of the intensity of the actions may be assumed.

As it is stated in the FIB model code 2010 [6], plastic analysis of beams, frames and slabs with the kinematic theorem without any check of the rotation capacity may be used for the ultimate limit state if all the following conditions are met:

- The area of tensile reinforcement is limited to such a value that at any section
 - $\frac{x_u}{d} \leq 0.25$ for concrete strength classes \leq C50;
 - $\frac{x_u}{d} \leq 0.15$ for concrete strength classes \geq C55;
- Reinforcing steel is either Class B or C;
- The ratio of the moments at intermediate supports to the moments in the span is between 0.5 and 2
- The ultimate moment M_u has to be always higher or equal to the moment of cracking M_f , to avoid brittle failure and therefore ensure a plastic rotation. As shown in the following Figure 26.

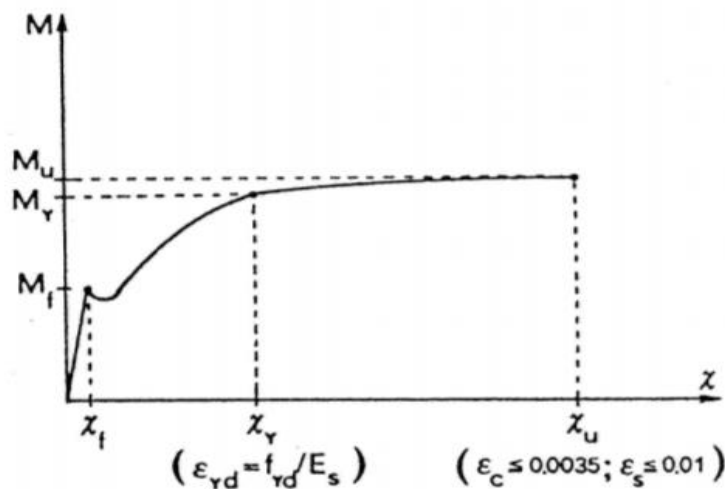


Figure 26: Moment vs curvature

3.1.1 Upper and lower bound theorems

Plastic analysis methods derive from the general theory of structural plasticity, which states that the collapse load of a structure lies between two limits, an upper bound and a lower bound of the true collapse load. These limits can be found by well-established methods. A full solution by the theory of plasticity would attempt to make the lower and upper bounds converge to a single correct solution. The lower bound theorem and the upper bound theorem, when applied to slabs, can be stated as follows:

- **Lower bound theorem:** If, for a given external load, it is possible to find a distribution of moments that satisfies equilibrium requirements, with the moment not exceeding the yield moment at any location, and if the boundary conditions are satisfied, then the given load is a lower bound of the true carrying capacity.

- **Upper bound theorem:** If, for a small increment of displacement, the internal work done by the slab, assuming that the moment at every plastic hinge is equal to the yield moment and that boundary conditions are satisfied, is equal to the external work done by the given load for that same small increment of displacement, then that load is an upper bound of the true carrying capacity.

If the lower bound conditions are satisfied, the slab can certainly carry the given load, although a higher load may be carried if internal redistributions of moment occurred. If the upper bound conditions are satisfied, a load greater than the given load will certainly cause failure, although a lower load may produce collapse if the selected failure mechanism is incorrect in any sense. Within the plastic analysis of structures, it should be considered either lower bound theorem or the upper one, not both, and precautions are taken to ensure that the predicted failure load at least closely approaches the correct value.

3.2 Yield Line Theory

One practical method for the plastic analysis of slabs is the Yield Line Theory [11]. This theory is an analysis approach for determining the ultimate load capacity of reinforced concrete slabs and was pioneered by K.W. Johansen in the 1940s. The yield line method of analysis for slabs is an upper bound method, and consequently, the failure load calculated for a slab with known flexural resistances may be higher than the true value. For this reason, the results are either correct or theoretically unsafe. It is possible to apply this theory only for ductile (under reinforced) slabs.

The *plastic hinge* that is located along a member in a continuous beam or frame at which, upon overloading, there would be a large inelastic rotation at essentially a constant resisting moment, for slabs this corresponding mechanism is the *yield line*. For the overloaded slab, the resisting moment per unit length measured along a yield line is constant as inelastic rotation occurs. The yield line serves as an axis of rotation for the slab segment. We assume that the following moment-rotation diagram holds, Figure 27.

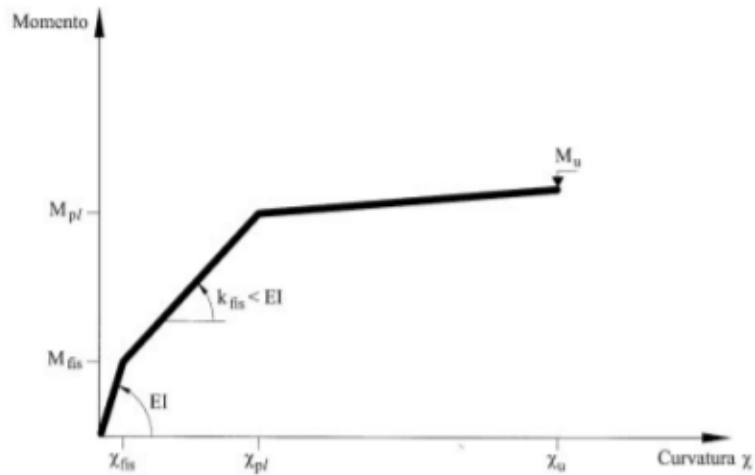


Figure 27: Ductile moment-rotation diagram [16]

The advantages of Yield Line over Linear Elastic Analysis are [11]:

- Simpler to use (computer not necessary);
- Linear elastic only tells you when the first yield occurs. Y.L. gives the ultimate capacity of the slab - what it takes to cause the collapse;
- Helps to understand ultimate behavior;
- Good for nonstandard shapes.

Disadvantages are:

- Requires experience in order to estimate the most likely failure mechanism because dangerous designs are possible without checking.
- Does not give an idea of slab behavior in service.

3.2.1 Yield line analysis proceeds

The design procedure should be started with estimation of the yield line pattern of the structure in question. There are strictly established rules for this task which could be found below (Figure 28):

- Yield lines divide the slab into rigid regions which remain plane through the collapse;
- Yield lines are straight lines because they represent the intersection of two planes.
- Axes of rotation generally lie along lines of support and pass over any column;
- Yield lines between adjacent rigid regions must pass through the point of intersection of the axes of rotation of those regions;
- Yield lines must end at a slab boundary;
- Continuous supports repel and a simple support attracts yield lines.
- Yield line forms under concentrated loads, radiating outward from the point of application.

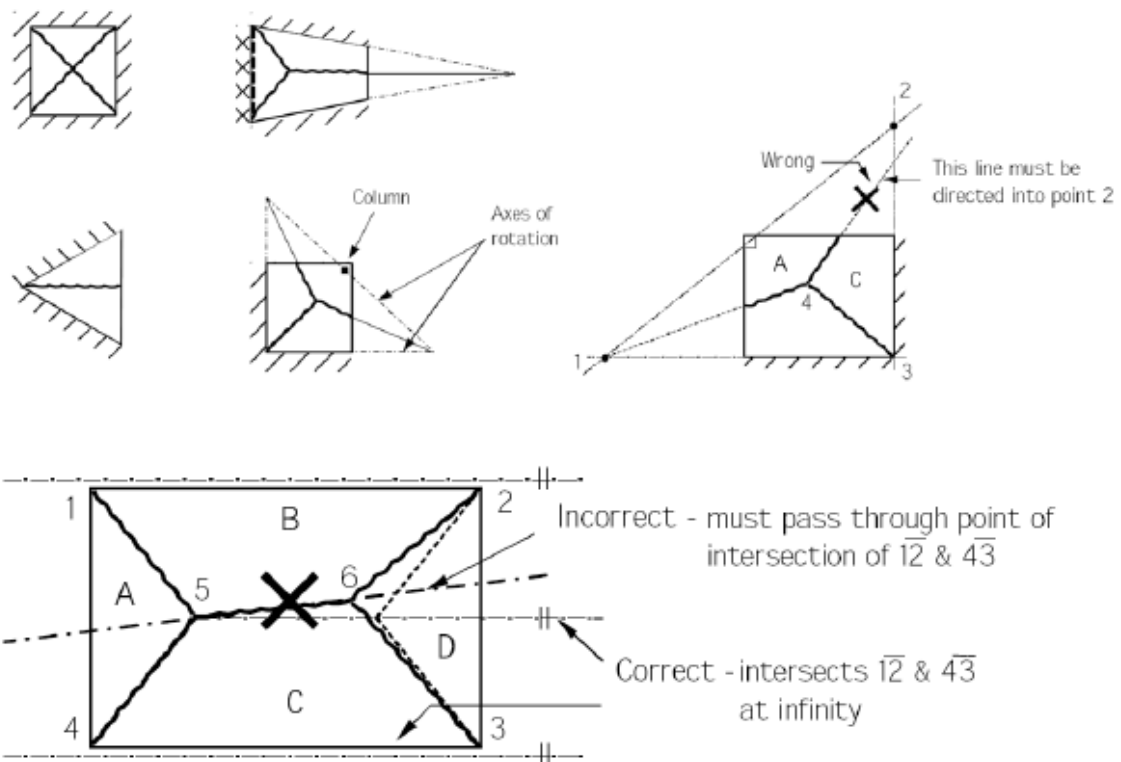


Figure 28 Example of rules for Yield Line [11]

As it was stated previously, firstly, the correct failure mechanism should be established by means of correct position of yield lines (Figure 29)

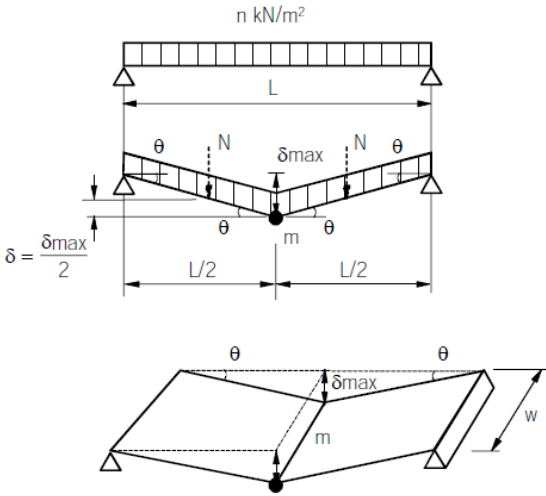


Figure 29 Example of collapse mechanism [12]

The virtual work method is used to calculate the ultimate load for yield line analysis. In the virtual work method, it is assumed that at failure there is no loss of energy in the slab, which means that the internal work is equal to the external one.

$$\begin{aligned}
 & \text{External work} = \text{Internal work} \\
 & \sum(N \cdot \delta)_{\text{for all regions}} = \sum(m \cdot l \cdot \theta)_{\text{for all regions}} \qquad (3.1)
 \end{aligned}$$

Where

- N is the load(s) acting within a particular region [kN or kN/m²]
- δ is the vertical displacement of the load(s) N on each region expressed as a fraction of unity [m]
- m is the moment or moment of resistance of the slab per metre run represented by the reinforcement crossing the yield line [kNm/m]
- l is the length of yield line or its projected length onto the axis of rotation for that region [m]
- θ is the rotation of the region about its axis of rotation [m/m]

The external work done is the total load on the slab times the average displacement it moves through; the internal work is the moment capacity of the yield line times the rotation it moves through along the length.

Once a valid failure pattern (or mechanism) has been postulated, either the moment, m , along the yield lines or the failure load of a slab, N (or indeed n kN/m²), can be established by applying the above equation.

So, the Yield line analysis proceeds in this way [12]:

- Quantifying External work

The external work is calculated by taking, in turn, the resultant of each load type (i.e. uniformly distributed load, line load or point load) acting on a region and multiplying it by its vertical displacement measured as a proportion of the maximum deflection implicit in the proposed yield line pattern. The total energy expended for the whole slab is the sum of the expended energies for all the regions.

- Quantifying internal work

The internal energy dissipated is calculated by taking the projected length of each yield line around a region onto the axis of rotation of that region, multiplying it by the moment acting on it and by the angle of rotation attributable to that region. The total energy dissipated for the whole slab, as for the external work, is the sum of the dissipated energies of all the regions.

- External work = Internal work

By using the equation 3.1, the value of the unknown i.e. either the moment, m , or the load, N , can then be established. If deemed necessary, several iterations may be required to find the maximum value of m (or the minimum value of load capacity) for each chosen failure pattern.

3.3 Application of Yield-Line Method for Elevated Slabs

According to ACI 544.6R-15 [4], the dominant failure mode for the flat slabs is to be produced by the a uniformly distributed load, with crack patterns that are characterized in two simplified mechanisms, as shown in Figure 30.

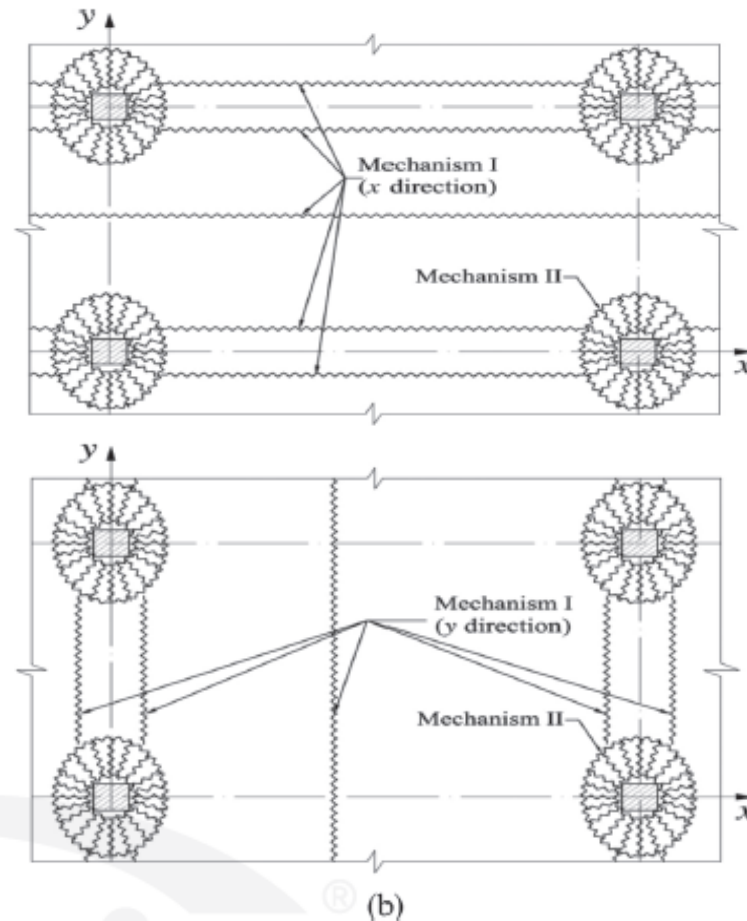


Figure 30 Crack patterns in elevated concrete slabs with Mechanism I - II formed in: (a) x-direction; and (b) y-direction,[4]

3.3.1 Mechanism I: global failure

The first collapse mechanism associated with flat slabs on a rectangular grid of columns are showed in the Figure 31. The fracture line pattern consists of parallel positive and negative moment lines with the negative yield line forming along the axis of rotation passing over a line of columns. This forms a folded plate type of collapse mode with maximum deflection taken as unity occurring along the positive yield line.

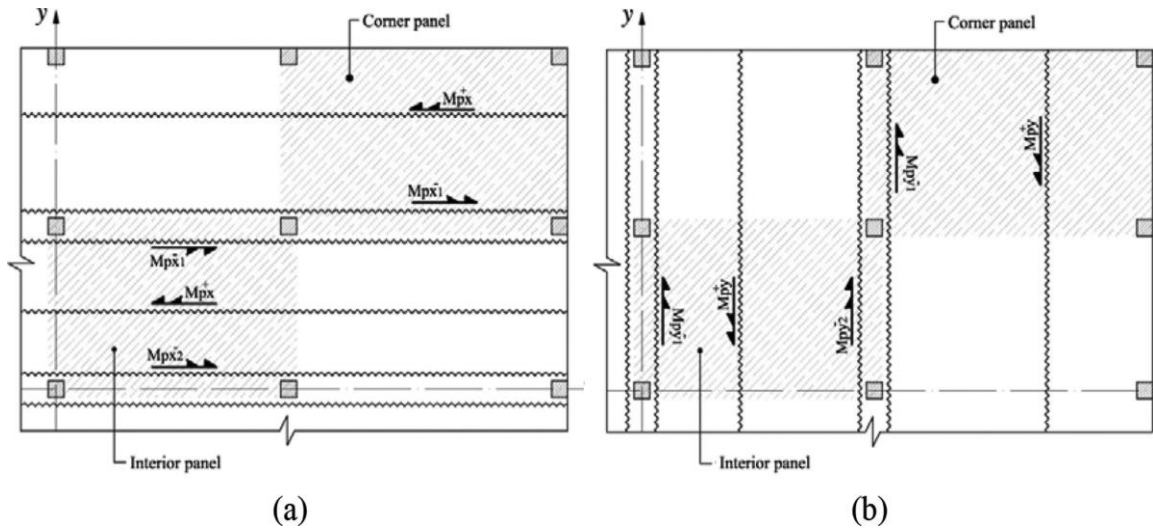


Figure 31 Yield line patterns for two most representative panels of E-SFRC slabs in: (a) x direction; and (b) y direction. [4]

Applying the principle of virtual work represented in Figure 32, the following equations are obtained:

$$M_{px}^+ = \frac{q_{ult} L_{ry}^2}{2(\sqrt{1+\Phi_{y1}} + \sqrt{1+\Phi_{y2}})^2} \quad (3.2)$$

$$M_{py}^+ = \frac{q_{ult} L_{rx}^2}{2(\sqrt{1+\Phi_{x1}} + \sqrt{1+\Phi_{x2}})^2} \quad (3.3)$$

Where M_{px}^+ is the slab's positive flexural strength in the y-direction, L_{rx} is the distance between two adjacent negative lines in one panel parallel to x-direction that may be assumed as indicated in fig. 6. The Φ_{x1} , Φ_{x2} , Φ_{y1} , and Φ_{y2} parameters in the previous equations result from assuming the general approach of having orthotropic reinforcement in both slab directions. In the case of steel fibre-reinforced concrete (SFRC) slabs, if a uniform fibre distribution is assumed in both directions of the slab, $\Phi_{x1} = \Phi_{x2} = \Phi_{y1} = \Phi_{y2} = \Phi_h$, the slab's positive and negative flexural strength can be calculated from the following equations:

$$M_{px}^+ = \frac{q_{ult} L_{ry}^2}{8(1+\Phi_h)} \quad (3.4)$$

$$M_{px}^- = \Phi_h M_{px}^+ \quad (3.5)$$

If a uniform distribution of fibres in the section Φ_h is assumed equal to 1.

$$M_{px}^+ = \frac{q_{ult}L_{ry}^2}{16}; M_{px}^- = M_{px}^+ \quad (3.6)$$

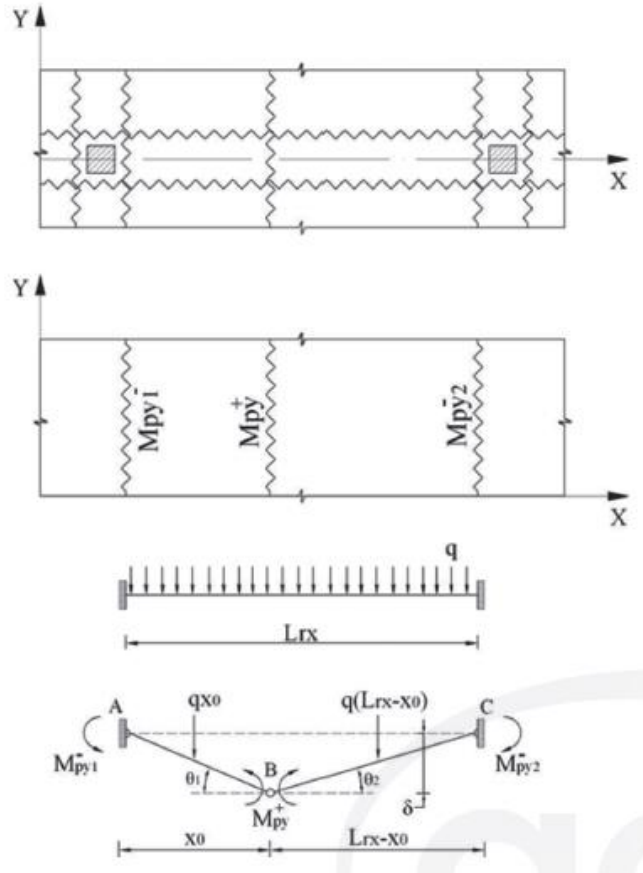


Figure 32: Principle of virtual work to estimate the ultimate load-carrying capacity of interior panel of slab submitted to uniform distributed load, [4]

Applying the yield-line theory for the panel at the corner of the slab, as shown in the figure 33, the following equations could be obtained:

$$M_{px}^+ = \frac{q_{ult}L_{ry}^2}{2(\sqrt{(1+\Phi_h)+1})^2} \quad (3.7)$$

If a uniform distribution of fibres in the section Φ_h is assumed equal to 1

$$M_{px}^+ = \frac{q_{ult}L_{ry}^2}{2(\sqrt{2+1})^2}; M_{px}^- = M_{px}^+ \quad (3.8)$$

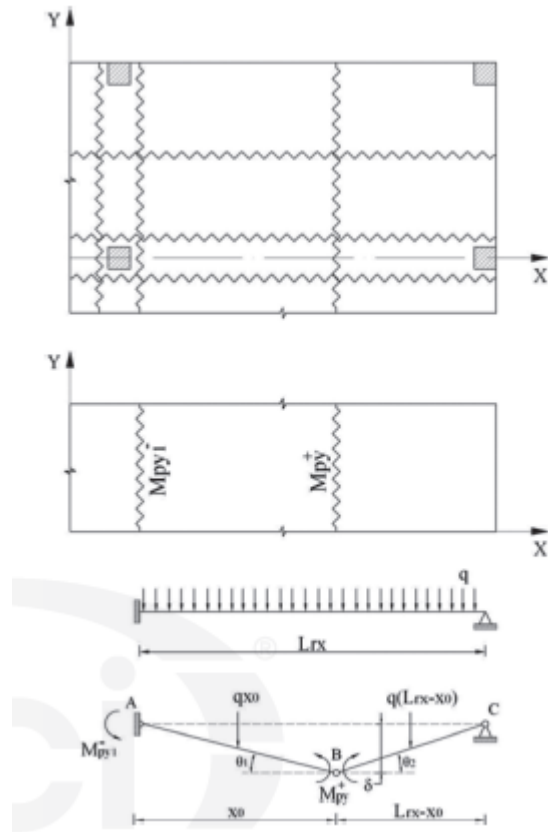


Figure 33: Principle of virtual work to determine ultimate load-carrying capacity of strip of interior panel of slab subjected to uniform distributed load and line load (parallel to yield lines).

For the case of a the elevated slab submitted to point load, positive yield lines propagate in a circular surface around the load point, whereas diagonal negative yield lines are formed in a so-called fan pattern, Figure 34. Positive and negative bending moments for point loading could be estimated by following equations:

$$M_p^+ = \frac{P \left(1 - \frac{2}{3} \frac{a}{R}\right)}{2\pi(1 + \Phi_h)} \quad (3.9)$$

$$M_p^- = \Phi_h M_p^+ \quad (3.10)$$

where P is the ultimate load distributed in an area of diameter a, and R is the radius of the negative yield line that can be calculated with respect to the column-to-column distances.

$$R = \sqrt{\frac{L_x L_y}{\pi}} \quad (3.11)$$

For the panel at the corner of the slab, the value of the moment for an internal panel should be divided by 2:

$$M_{p,corner}^+ = \frac{M_{p,internal\ panel}^+}{2} \tag{3.12}$$

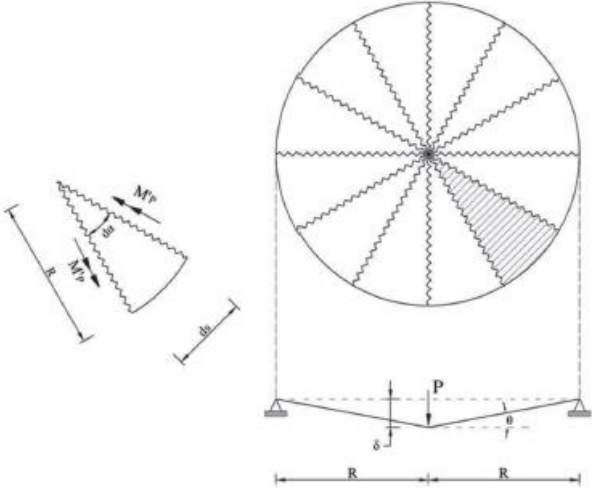


Figure 34: Principle of virtual work to calculate flexural strength of elevated slab submitted to point load [4]

3.3.2 Mechanism II: Local failure

The second mechanism is a local failure that should be considered for the ground slabs and also for the elevated floors supported by discontinued piles or columns. Punching shear failure can be considered as an extra criteria to design this type of slab.

Local flexural failure mechanism consists of the negative yield lines emanate from the column and a positive circumferential yield line forms at the bottom of the cone shaped surface (Figure 35). The ellipse axes dimensions are affected by the dimensions of the column cross section (a, b) and the respective spans of the structure (Lx and Ly):

$$r_x = 0,65L_x \sqrt[3]{\frac{a}{L_x}} \tag{3.13}$$

$$r_y = 0,65L_y \sqrt[3]{\frac{b}{L_y}} \tag{3.14}$$

3.4 Flexural strength of FRC element

FIB Model Code constitutive laws for FRC were studied for analysis of concrete elements in question. Within the thesis the structural behaviour in the ultimate limit state was deeply studied, therefore the rigid-plastic model was applied [6]. Steel fibre reinforced concrete is assumed to have an ideally-plastic behavior, where the ultimate residual strength f_{Ftu} , could be calculated through the following equation:

$$f_{Ftu} = \frac{f_{R3k}}{3\gamma_F} \quad (3.19)$$

For bending moment and axial force in the ultimate limit state, a simplified stress/strain relationship is given by the FIB model code. The simplified stress distributions can be seen in Figure 34. where the linear post cracking stress distribution is to the left and the rigid plastic stress distribution is to the right. The rectangular stress block was assumed for the zone subjected to compression, taking into consideration the following parameters: $\eta = 1$ and $\lambda = 0.8$ for concrete with compressive strength below or equal to 50 MPa. Also, the residual flexural tensile strength of the fibres is added as a stress block as it possible to appreciate in Figure 36, considering a safety factor $\gamma_F = 1.5$ it should be noticed that the safety factor.

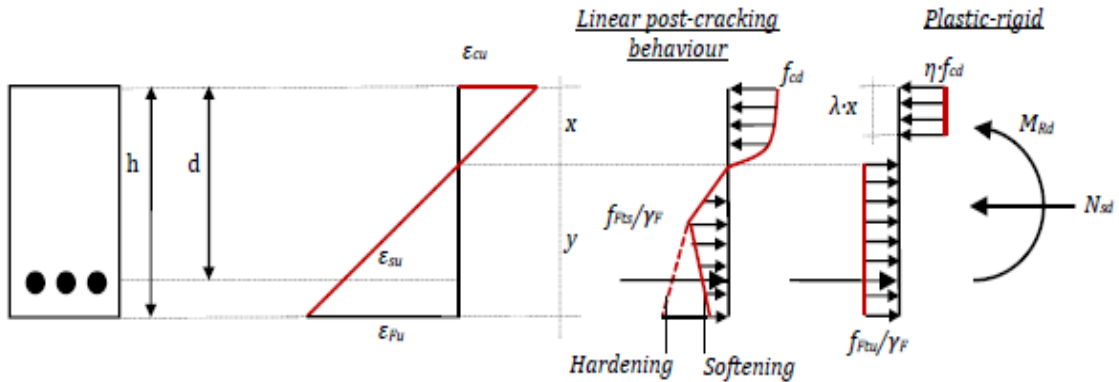


Figure 37: Simplified stress/strain relationship including the residual flexural tensile strength of fibres [6]

The ultimate resistant moment was calculated using the rotation equilibrium equation around the point where compression force is acting:

$$Mrd = f_{yd}A_s \left(d - \frac{\lambda x_u}{2} \right) + f_{tu}B(H - x_u) \left(\frac{H - x_u}{2} + \left(1 - \frac{\lambda}{2} \right) x_u \right) \quad (3.20)$$

where

$f_{yd} = \frac{f_{yk}}{\gamma_s}$ is the design yield strength of steel rebars [KN/m²]

$\gamma_s = 1.15$ is the material safety factor of steel rebars [-]

A_s is the area of the traditional reinforcement [m²]

H is depth of the slab [m]

x_u is the height of compressive stress block in the ultimate limit state [m]

d is the effective depth of the bars [m]

B is the width of the section. Here, B=1 [m]

The value of the neutral axis, in turn, was calculated using the translation equilibrium equation

$$C = T \rightarrow f_{cd}B\lambda x = f_{tu}B(H - x) + f_{yd}A_s \rightarrow x = \frac{f_{tu}B(H-x) + f_{yd}A_s}{f_{cd}B\lambda} \quad (3.21)$$

3.5 The arrangement of steel reinforcement

3.5.1 Top reinforcement

For the positioning of the top reinforcement, a positioning criteria was used in the Practical Yield Line Design [12]. According to Yield Line principles, the total bay moment is taken into account regardless of whether the reinforcement is distributed over the whole bay or concentrated over only part of it. Yield Line Design, therefore, allows designers to choose if they wish, other arrangements of reinforcement. According to Yield Line principles, the moment resistant given by top steel reinforcement could be distributed over the whole span or concentrated over only part of it. In the latter case there are advantages if the concentration is around the column, in particular the improvement of:

- Shear resistant, in cases of local failure and punching failure;
- Sending moment resistant at the head of the column, where you have peaking values due to service loads.

The common concentrations of top reinforcement over columns when using Yield Line Design are shown in the following table.

Location of column	Reinforcement concentrated in the <u>area</u> of dimensions		
	x (or y)		y (or x)
Internal	0.5 L	x	0.5 L
Edge	0.5 L	x	(0.2 L + E.D.)
Corner	(0.2 L + E.D.)	x	(0.2 L + E.D.)

Table 5: Common concentrations of top reinforcement over columns when using Yield Line Design, where E.D.= edge distance is the centerline of the column to the edge of slab and L is the length of the span. [12]

For resistance to local failure and punching shear failure, top reinforcement is best concentrated around the column.

The curtailment criteria of top reinforcement, in Yield Line Design, are not governed by conventional rules used in Elastic Design, but by the configuration of the crack patterns and collapse mechanism. So once collapse mechanism is established, the designer has to be careful that the steel reinforcement concentration doesn't produce a new failure pattern at lower loads.

For the general case for flat slabs, when the spans are approximately equal, loads are predominately uniformly distributed loads and the design has been carried out using the single

load case of maximum design load on all spans. Then 100% top steel may generally be curtailed at $0.25 \times \text{span}$ from the centerline of internal columns and 100% top steel may generally be curtailed at a distance of $0.20 \times \text{span}$, at right angles to the edge, from the centerline of perimeter columns.

3.5.2 Bottom reinforcement

The bottom reinforcement, using Yield Line Design principles, is assumed generally regular in whole bays for the slab, without curtailment. That curtailment of bottom reinforcement is best avoided because it is usual to assume a constant moment along the whole length of the yield lines.

In Yield Line Design, the checks involving the localised failure modes around column supports use the full moment of resistance of the bottom reinforcement within the areas of the local failure patterns. It is therefore advisable not to carry out any curtailment of bottom bars in these areas.

It may then be necessary to check whether a yield line pattern giving a lower overall load capacity can develop along the line where the reinforcement is reduced.

Moreover, conventional detailing practice following the bending moment envelope leads to inefficiencies in production due to:

- Different length bars increase the number of bar marks and impose a strict discipline on their placing.
- Staggering bars of the same length also slows down the laying process.
- Changing bar diameters and their spacing to fit as closely as possible to the moment will also effect the time needed to place the bars.
- Complex reinforcement layouts also require more checking and offer very little flexibility.

All these points incur increased labour costs and slow down progress on site. So, for Yield Line designs it is recommended that bottom steel reinforcement is not curtailed, and it is positioned over the entire length of the slab span.

3.6 Punching shear in SFRC

The steel fibres in concrete can also considerably influence shear behavior and shear capacity. Fibres can reduce the amount of stirrups and congestion of reinforcement in high shear regions. Fibres do not only improve the flexural behavior but also the shear capacity. [13]

In flat slabs, punching shear failures normally develop around supported areas (columns, capitals, walls). Punching can also result from a concentrated load applied to a relatively small area of the structure.

The design procedure for punching shear is based on checks at the face of the column and at the basic control perimeter u_1 . If shear reinforcement is required a further perimeter $u_{out,ef}$ should be found where shear reinforcement is no longer required. How it is explained in the Eurocode [14], the following checks should be carried out:

- At the column perimeter, or the perimeter of the loaded area, the maximum punching shear stress should not be exceeded:

$$v_{Ed} < v_{Rd,max} \quad (3.22)$$

- Punching shear reinforcement is not necessary if:

$$v_{Ed} < v_{Rd,F} \quad (3.23)$$

Where

$v_{Rd,F}$ is the design value of the punching shear resistance of a slab without punching shear reinforcement along the control section considered.

$v_{Rd,max}$ is the design value of the maximum punching shear resistance along the control section considered.

v_{Ed} is the maximum shear stress agent.

From a practical point of view, the influence of SFRC for shear resistance is mainly related to the possibility of replacing all transverse reinforcement. In the “fib bulletin 57 Shear and Punching Shear in RC and FRC Elements” [13], the equation suggested by Eurocode 2 to compute the shear contribution in concrete members without shear reinforcement, was modified to include the influence of fibres

The design punching shear resistance [MPa] of a FRC slab without punching shear reinforcement was rearranged by adding the term $\frac{f_{Ftuk}}{\gamma_F}$ and may be calculated as follows:

$$v_{Rd,F} = v_{Rd,c} + v_{Rd,f}$$

$$v_{Rd,F} = C_{Rd,c} k (100 \rho_l f_{ck})^{\frac{1}{3}} + k_1 \sigma_{cp} + \frac{f_{Ftuk}}{\gamma_F} \quad (3.24)$$

where:

f_{ck} is compressive strength in MPa

σ_{cp} is the average stress acting on the concrete due to loading or prestressing.

f_{Ftuk} is the characteristic value of the ultimate residual tensile strength for FRC, by considering $w_u = 1.5$ mm [MPa]

f_{ctk} is the characteristic value of the tensile strength for the concrete matrix. [MPa]

$$k = 1 + \sqrt{\frac{200}{d}} \leq 2, \text{ d in mm}$$

$$C_{Rd,c} = \frac{0.18}{\gamma_c}$$

$\rho_l = \sqrt{(\rho_{lx} \cdot \rho_{ly})} \leq 0.02$, and ρ_{lx} , ρ_{ly} relate to the bonded tension steel in x- and y- directions respectively. The values ρ_{lx} , ρ_{ly} should be calculated as mean values taking into account a slab width equal to the column width plus 3d each side.

The code also defines a minimum value for the shear resistance, which is given by the following equation

$$v_{min} = 0.035 k^{\frac{3}{2}} f_{ck}^{\frac{1}{2}} \quad (3.25)$$

The shear resistance $v_{Rd,max}$ is the maximum of the value $v_{Rd,c} - v_{min}$

If v_{Ed} exceeds the value $v_{Rd,c}$ for the control section considered, punching shear reinforcement should be provided according the Eurocode. The design procedure for punching shear is based on checks at the face of the column u_0 . and at the basic control perimeter u_1 . The maximum shear stress should be taken as:

$$v_{ed} = \frac{\beta v_{ed}}{u_{0,1} d} \quad (3.26)$$

Where

V_{ed} is the acting reaction in the column minus the agent external loads in the perimeter u_1

$u_{0,1}$ is the basic control perimeter

d is the mean effective depth of the slab

β is a parameter that recommended values are given in Figure 37

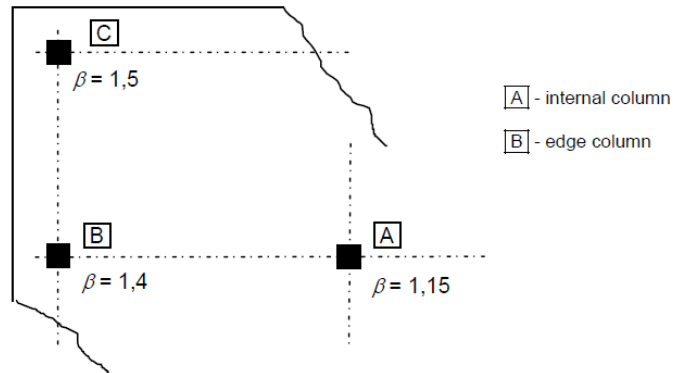


Figure 38: Recommended values for β

The basic control perimeter u_1 may normally be taken to be at a distance $2d$ from the loaded area and should be constructed to minimise its length. It is possible to calculate it as shown in the figure 38

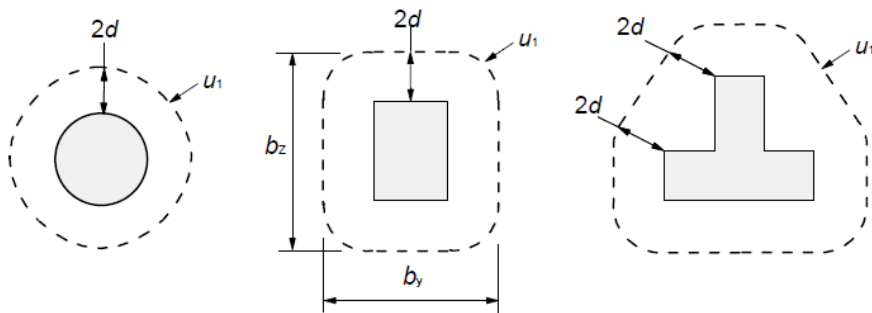


Figure 39: Typical basic control perimeters around loaded areas

Where shear reinforcement is required $v_{Ed} > v_{Rd,c}$, it should be calculate the area of the reinforcement in accordance with Eurocode 2:

$$v_{Rc,cs} = 0.75v_{Rd,c} + 1.5 \left(\frac{d}{s_r} \right) A_{sw} f_{ywd} \left(\frac{1}{u_1 d} \right) \sin \alpha \quad (3.27)$$

Where:

A_{sw} is the area of one perimeter of shear reinforcement around the column [mm²]

s_r is the radial spacing of perimeters of shear reinforcement [mm]

$f_{ywd} = 250 + 0.25d \leq 400$ is the effective design strength of the punching shear reinforcement. [MPa]

α is the angle between the shear reinforcement and the plane of the slab.

Through the following equation (3.28) is possible to calculate the control perimeter at which shear reinforcement is no required.

$$u_{out,ef} = \frac{\beta V_{ed}}{v_{Rd,cd}} \quad (3.28)$$

4 Parametric studies

Parametric studies are aimed to analyse the influence of the SFRC in a flat slab. It is carried out some parametric studies aimed to analyse the influence of the compressive and tensile strength of the fibre reinforced concrete on flexural behavior. The ratio between the negative and positive area of ordinary reinforcement is analysed to verify if it affects the total amount of steel. At the end, it is studied the redistribution percentage of an elastic moment for different cases.

It is important first of all to define the model, so the stage consists of the following previous steps:

- Flat slab's dimension, which can be arbitrarily set.

As a first example, it has been defined a quadratic 4x4 slab. It is considered a length of 6 meters for each span in both directions, thus obtaining 6x6m square panel. Pillars with dimensions of 25 x 25 cm were also considered.

- Choice of the slab thickness (t) in order to limit the slab slenderness (t/L =thickness/span length) in the range:

$$\frac{1}{35} \leq \frac{t}{L} \leq \frac{1}{25}$$

So it's defined a thickness of 200 mm

- Definition of material properties:

The material properties of the concrete and steel reinforcement are summarized in table 6 and 7. B500C steel and a C50/60 concrete are considered.

Conventional reinforcing steel		
Designation	Unit	B500C
Modulus of elasticity E_s	[MPa]	210000
Characteristic yielding strength f_{yk}	[MPa]	500
Safety factor γ_s	[-]	1,15
Design yielding strength f_{yd}	[MPa]	434,7826
Specific weight γ_g	[kg/m ³]	7850

Table 6: Conventional reinforcing steel properties

Concrete		
Designation	Unit	
Mean modulus of elasticity E_{cm}	[MPa]	38629
Poisson's coefficient	[-]	0,15
Characteristic cylindrical compressive strength f_{ck}	[MPa]	50
Safety factor γ_c	[-]	1,5
Design compressive strength f_{cd}	[MPa]	33,3
Mean tensile strength f_{ctm}	[MPa]	4,07
Mean flexural tensile strength $f_{ctm,fl}$	[Mpa]	5,7

Table 7: Concrete properties

In this thesis, for the tensile contribution of the concrete given by the fibres, the values obtained from a study carried out at the University of Brescia for a technical paper [12] are used. The following table shows the values of tensile strength for different quantities of fibres. From the value f_{R3k} is possible to calculate the ultimate residual strength f_{Ftu} by the equation (3.19)

Fibre dosage	Fibre aspect ratio	Fibre tensile strength	F_{r3k}	F_{tu}
[Kg/m ³]	[-]	[GPa]	[Mpa]	[Mpa]
0	80	2	0	0
15			2,1	0,46
20			2,7	0,6
25			3,4	0,75
30			4,1	0,91
40			5,5	1,22
50			6,9	1,53
60			8,2	1,82
70			9,6	2,13

Table 8: Fibre properties [15]

- Set the arrangement of the rebars

As already explained in chapter 3.5, the following arrangement in figure 39 has been taken into account for the top reinforcement. While the bottom reinforcement is arranged over the entire area of the slab.

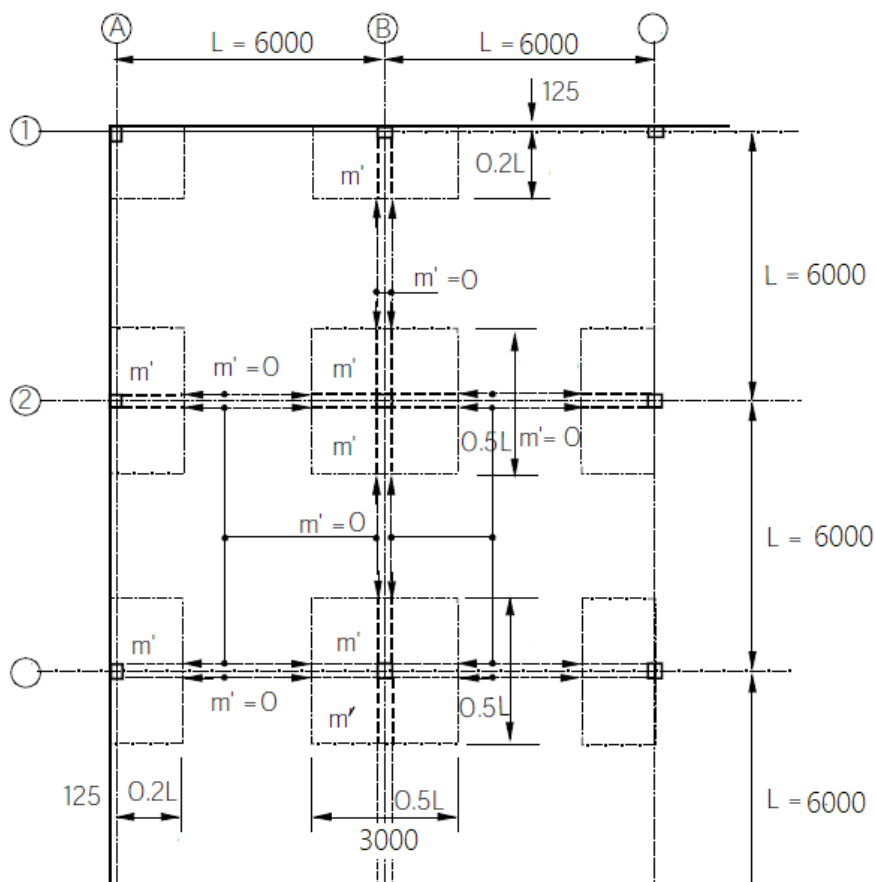


Figure 40: Proposed distribution of top of reinforcement [12]

- Cross section

The values of resistant moment obtained refer to one meter of length of the slab and it is considered a rebar covering of 30 cm, as shown in figure 40

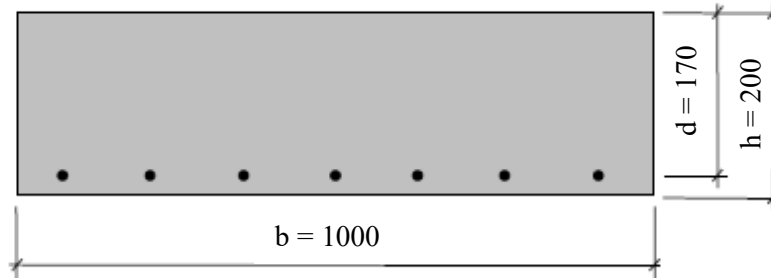


Figure 41: Cross section

- Define the cracking moment

$$M_{cr} = \frac{bh^2}{6} f_{ctm,fl} = 38 \left[\frac{KNm}{m} \right]$$

Once the parameters of the model are defined, some studies are aimed to analyse different important aspect.

4.1 Influence of f_{ck}

First of all, it is important to point out that the compressive strength of concrete does not significantly affect the behaviour and flexural resistance of the slab, with and without the ordinary reinforcement. Through equations 3.7, 3.20 and 3.21 the values of the ultimate resistant moment and the ultimate agent load are obtained. Two different values of compressive strength equal to 30 and 50 MPa are considered. It's showed that starting from about values of f_{R3k} higher than 6, there is a slight variation in the results. As the graph in Figure 41 shown, for value of $f_{R3k} = 9.6$, corresponding to 70 kg/m^3 of fibres, there is a variation of about 2 KNm^2 for the moment and therefore about 0,5 MPa for the ultimate load.

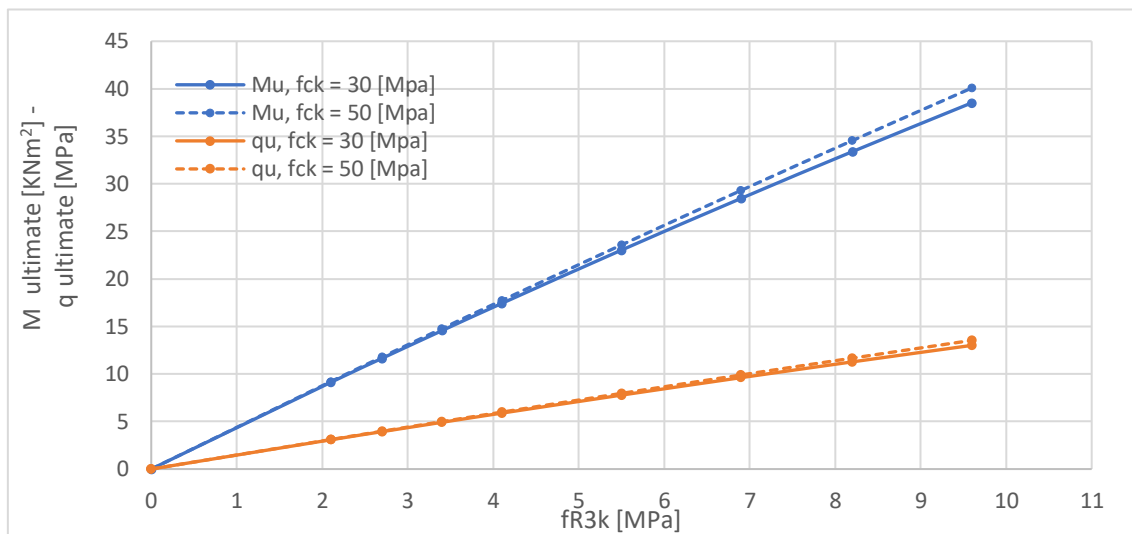


Figure 42: Mu – qu vs fR3k

It is clearly illustrated by the above graphs how the contribution of the fibres significantly influences the flexural strength, due to its traction contribution. In fact, as the residual tensile strength increases, the ultimate load that the slab can resist increases. It's also possible to notice that with a value of $fR3k=9,6$ it is possible to obtain the ultimate moment value equal the cracking moment.

Then, as shown in table 9, two different percentage of ordinary reinforcement are considered.

Bottom	Top	As,b [mm ² /m]	As,t [mm ² /m]	As,t/As,b [-]	$\rho_{s,b}$ [‰]	$\rho_{s,t}$ [‰]	f_{ck} [MPa]	CODE
Φ12/200	Φ12/200	565,5	568,5	1	2,82	2,82	30	2,82/30
Φ12/200	Φ12/200	565,5	568,5	1	2,82	2,82	50	2,82/50
Φ14/200	Φ14/200	769,7	769,7	1	3,84	3,84	30	3,84/30
Φ14/200	Φ14/200	769,7	769,7	1	3,84	3,84	50	3,84/50

Table 9: Cases studied

The results obtained show that if reinforcement bars are present in the slab, the compressive strength of the fibre-reinforced concrete has a slight influence when the percentage of reinforcement increases, but it can be considered negligible. The following graphs, in Figure 42 and 43, show the results obtained.

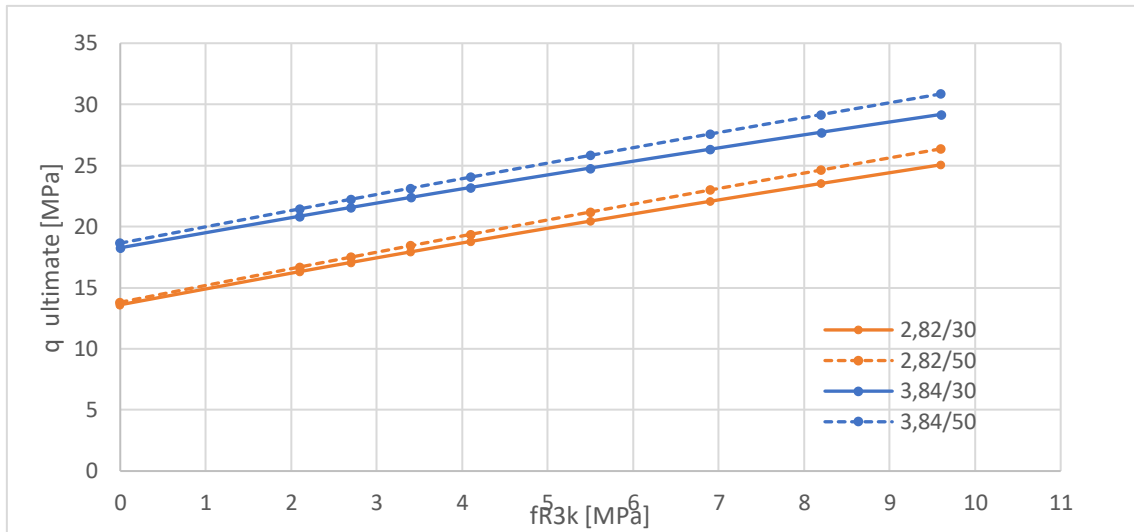


Figure 43: q_u vs f_{R3k}

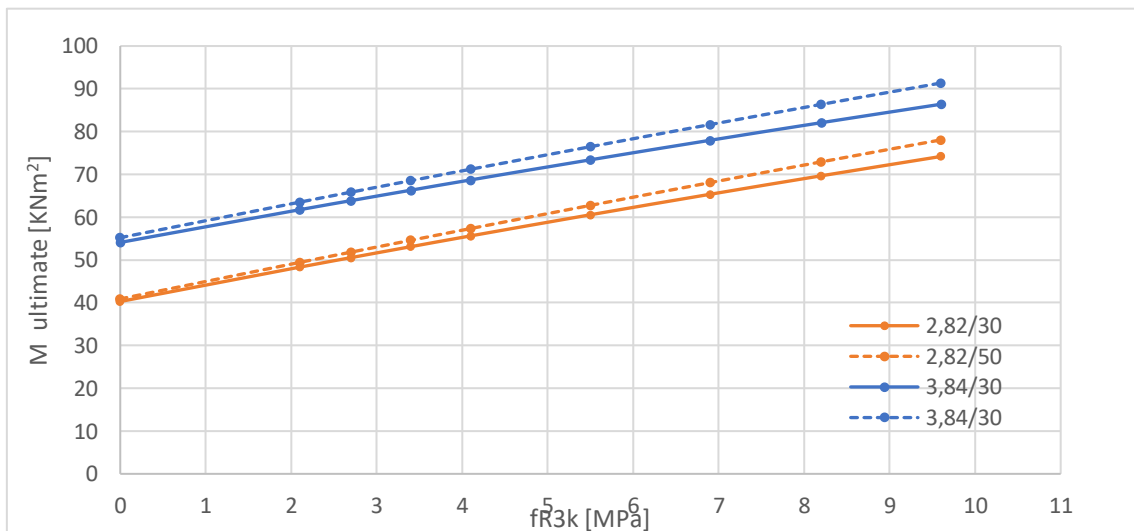


Figure 44: M_u vs f_{R3k}

In conclusion, the compressive strength doesn't affect the flexural behaviour of a SFRC, but its influence on fibre anchorage with the concrete matrix, so for the further studies it is considered a compressive strength $f_{ck} = 50$ MPa.

4.2 Influence of f_{R3k}

Keeping the same properties of the model, this study is aimed to analyse the influence of the flexural strength and the reinforcement area ratio. It is predefined a bottom reinforcement equal

to $\Phi 12/200$ and it is placed in the whole slab. While, a different top reinforcement is considered in order to obtain a different area ratio, as shown in the table 10

Bottom	Top	$A_{s,b}$ [mm ² /m]	$A_{s,t}$ [mm ² /m]	$A_{s,t}/A_{s,b}$ [-]	$\rho_{s,b}$ [%]	$\rho_{s,t}$ [%]	f_{ck} [MPa]	CODE
$\Phi 12/200$	$\Phi 12/200$	565,5	565,5	1	2,82	2,82	50	2,82/2,82-1
$\Phi 12/200$	$\Phi 14/200$	565,5	769,7	1,36	2,82	3,84	50	2,82/3,84-1,36
$\Phi 12/200$	$\Phi 16/200$	565,5	1005,3	1,77	2,82	5,02	50	2,82/5,02-1,77
$\Phi 12/200$	$\Phi 18/200$	565,5	1272,3	2,25	2,82	6,36	50	2,82/6,36-2,25
$\Phi 12/200$	$\Phi 20/200$	565,5	1570,8,6	2,77	2,82	7,85	50	2,82/7,85-2,77

Table 10: Cases studied

From the results obtained in Figure 44, it is easy to notice that it is possible to reach a predefined ultimate load by changing the following 2 parameters:

- Ratio A_{s^-}/A_{s^+}
- f_{R3k}

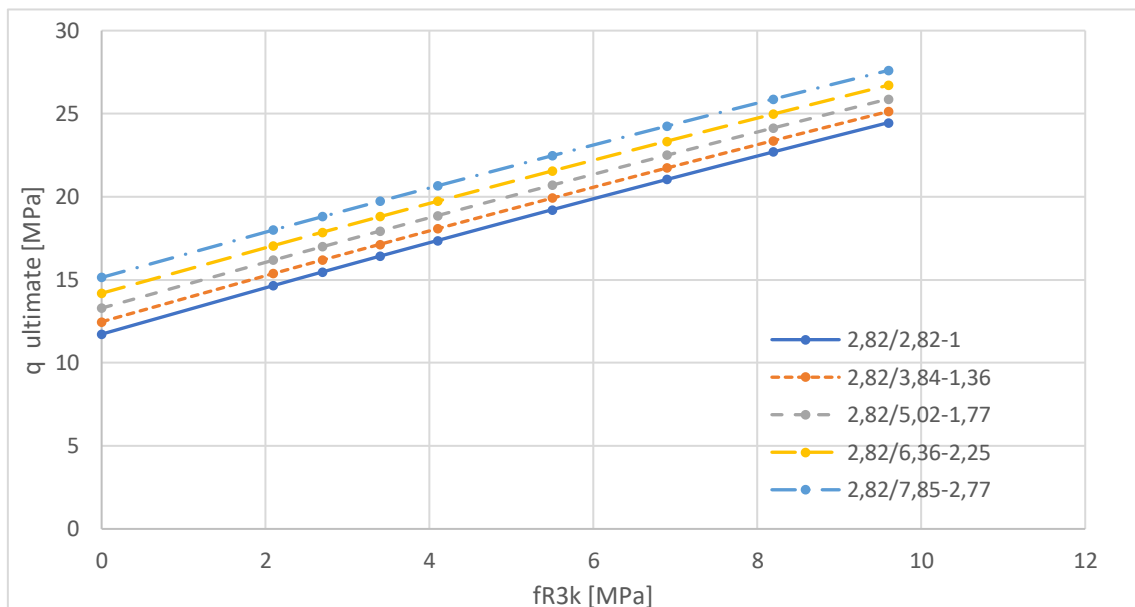


Figure 45: Graph ultimate load q_u vs F_{R3k}

In the graphs below (Figure 45 and 46), instead, it is calculated the depth of the neutral axis and the ratio between the moments M^-/M^+ , in order to verify if the results are within the limits (chapter 3.1).

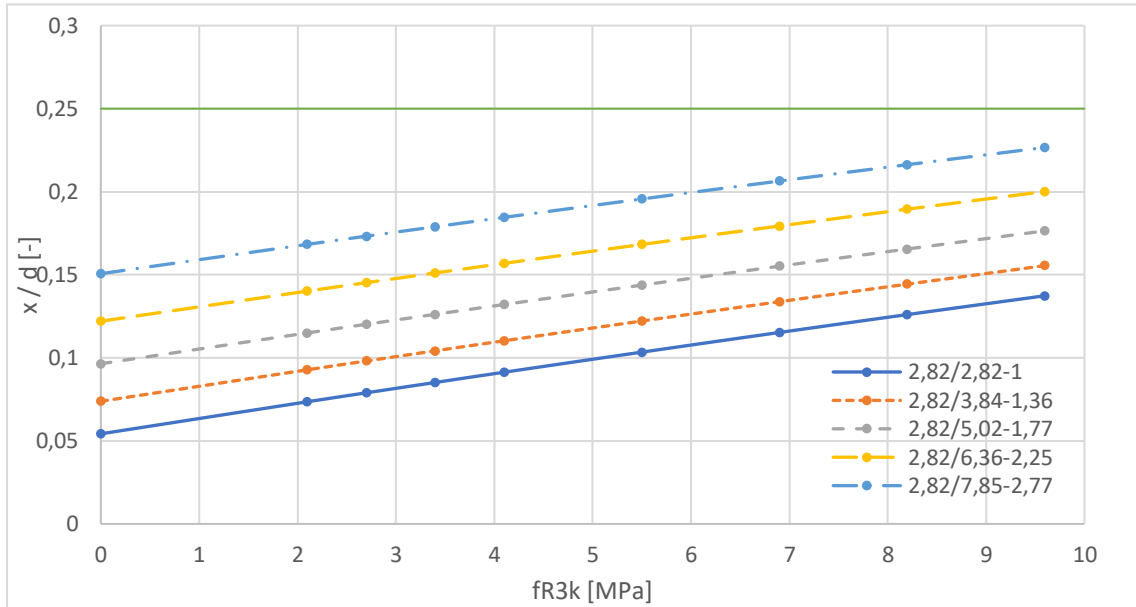


Figure 46: Graph ratio x/d vs f_{R3k}

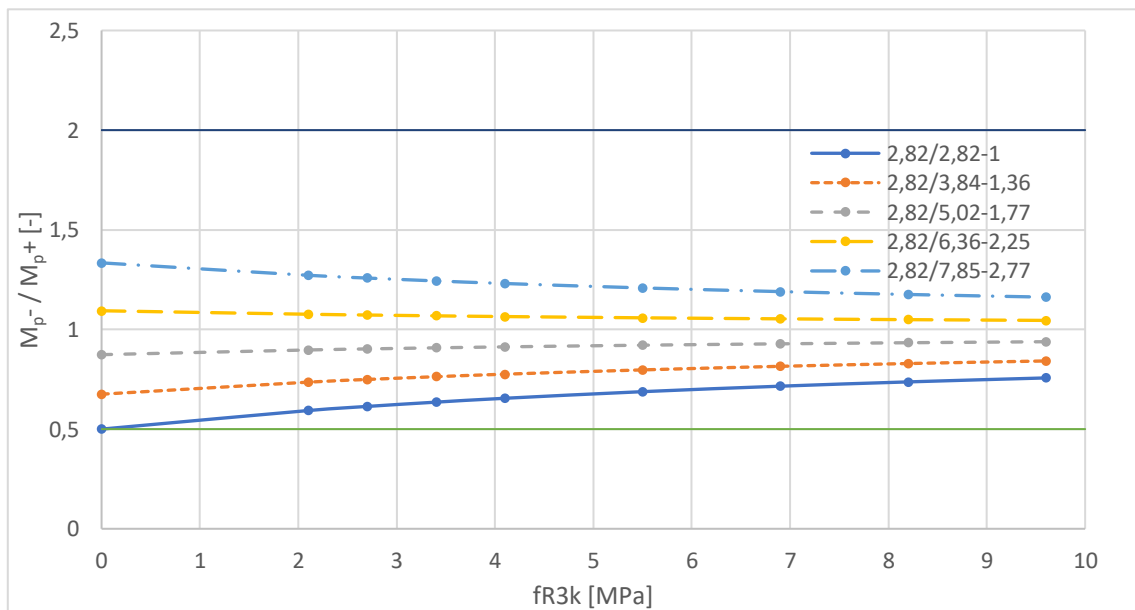


Figure 47: Graph ratio M_{p-} / M_{p+} vs f_{R3k}

4.3 Influence of As^-/As^+

The main scope of the thesis is to optimize the amount of steel reinforcement in a flat slab, so this study is aimed to analyse how the reinforcement area ratio influences the total amount of rebars. How it is illustrated in table 11, this analysis is carried out for a determinate quantity fibre (20 kg/m^3 and 40 kg/m^3) into the concrete and it is considered different bottom reinforcement with three different ratios of areas. Also, in this study case, the limitations and rules of construction present in the technical codes (chapter 3.1) are taken into consideration.

Bottom	As,b [mm ² /m]	As,t [mm ² /m]	$As,t/As,b$ [-]	$\rho_{s,b}$ [%o]	$\rho_{s,t}$ [%o]	f_{R3k} [MPa]	% Fibre content	CODE
Φ10/200	392,7	392,7	1	1,96	1,96	2,7	0,83	1-2,7-0,83
Φ10/150	549,7	549,7	1	2,74	2,74			
Φ12/200	565,5	565,5	1	2,82	2,82			
Φ14/200	791,7	791,7	1	3,95	3,95			
Φ16/200	1005,3	1005,3	1	5,02	5,02			
Φ10/200	392,7	785,4	2	1,96	3,92	2,7	0,83	2-2,7-0,83
Φ10/150	549,7	1099,6	2	2,74	5,49			
Φ12/200	565,5	1131	2	2,82	5,65			
Φ14/200	791,7	1539,4	2	3,95	7,69			
Φ16/200	1005,3	2010,6	2	5,02	10,0			
Φ10/200	392,7	1570,8	4	1,96	7,85	2,7	0,83	4-2,7,0,83
Φ10/150	549,7	2199,1	4	2,74	10,9			
Φ12/200	565,5	2261,9	4	2,82	11,3			
Φ14/200	791,7	3078,7	4	3,95	15,4			
Φ16/200	1005,3	4021,2	4	5,02	20,1			
Φ10/200	392,7	392,7	1	1,96	1,96	5,5	1,66	1-5,5-1,66
Φ10/150	549,7	549,7	1	2,74	2,74			
Φ12/200	565,5	565,5	1	2,82	2,82			
Φ14/200	791,7	791,7	1	3,95	3,95			
Φ16/200	1005,3	1005,3	1	5,02	5,02			
Φ10/200	392,7	785,4	2	1,96	3,92			
Φ10/150	549,7	1099,6	2	2,74	5,49			

Φ12/200	565,5	1131	2	2,82	5,65	5,5	1,66	2-5,5-1,66
Φ14/200	791,7	1539,4	2	3,95	7,69			
Φ16/200	1005,3	2010,6	2	5,02	10,0			
Φ10/200	392,7	1570,8	4	1,96	7,85	5,5	1,66	4-5,5-1,66
Φ10/150	549,7	2199,1	4	2,74	10,9			
Φ12/200	565,5	2261,9	4	2,82	11,3			
Φ14/200	791,7	3078,7	4	3,95	15,4			
Φ16/200	1005,3	4021,2	4	5,02	20,1			

Table 11: Case studied

Interesting results have been obtained, which will be listed below, figure 46, 47 and 48.

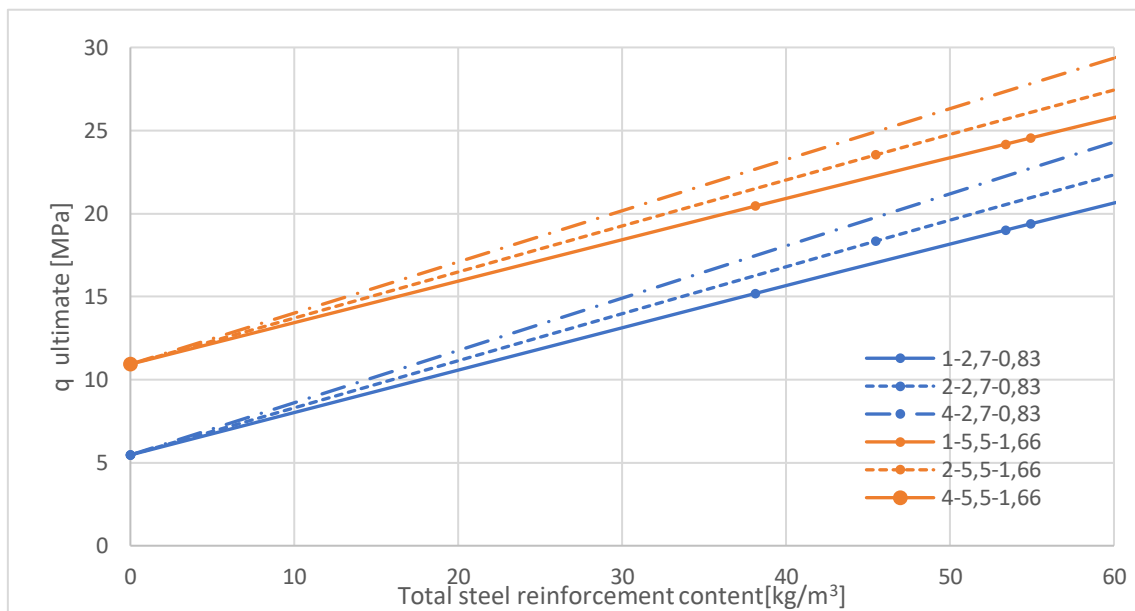


Figure 48: Graph ultimate load q_u vs Total steel reinforcement content [kg/m³]

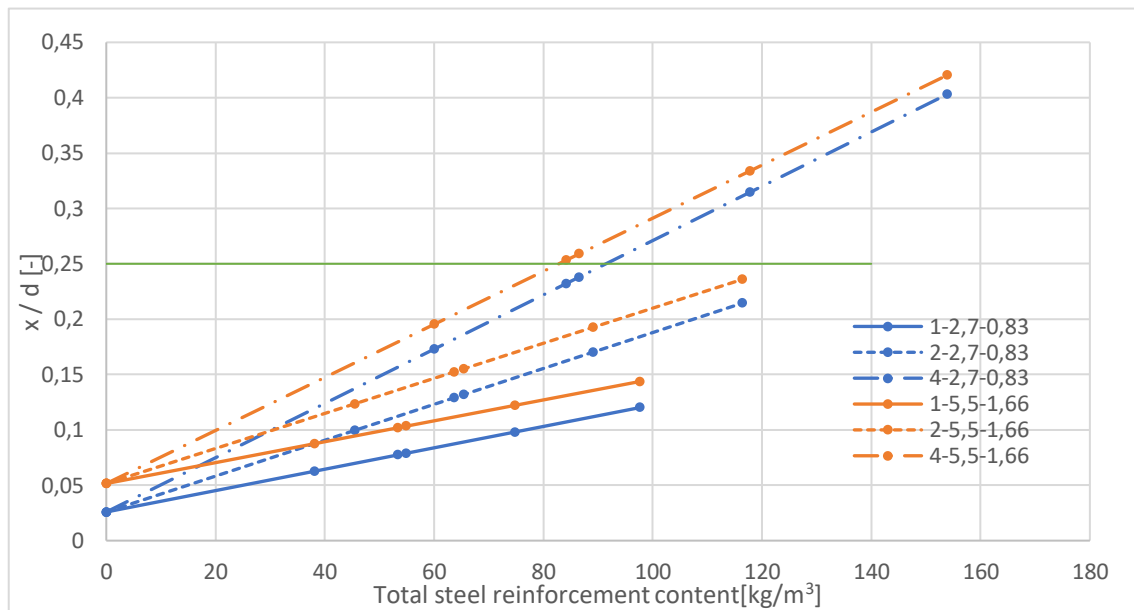


Figure 49: Graph ultimate load x/d vs Total steel reinforcement content [kg/m³]

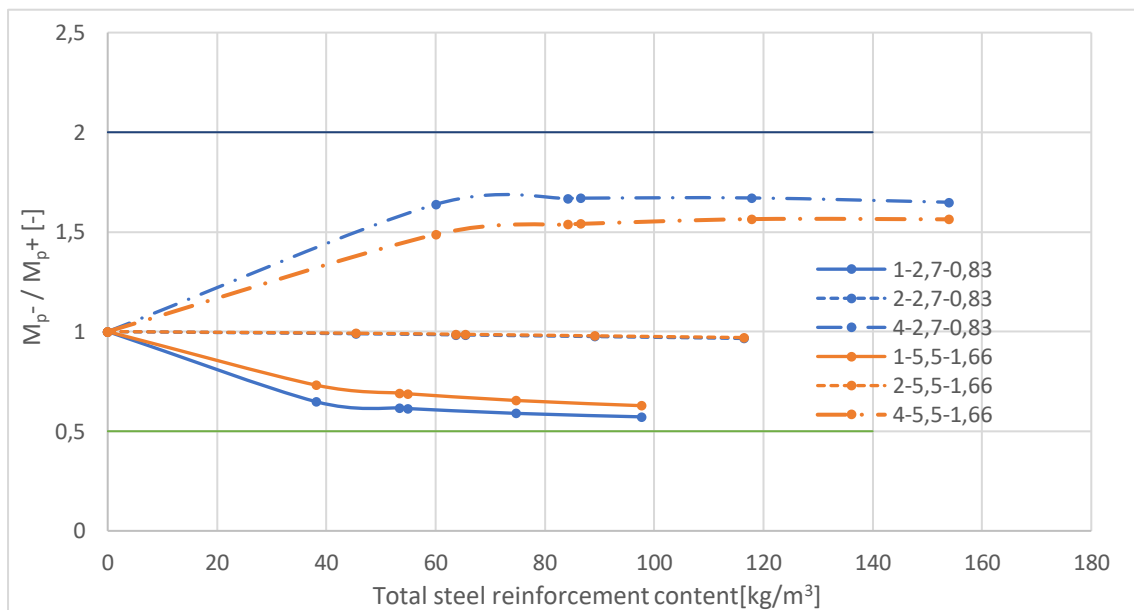


Figure 50: Graph ultimate load $M_{p-} / M_{p+} [-]$ vs Total steel reinforcement content [kg/m³]

In the above graphs, it is possible to highlight a relevant aspect. A different ratio between the negative and positive area of reinforcement influence the total amount of steel into the slab and obviously the value of the ultimate load that it is possible to resist.

It can be seen from the graphs obtained that for higher ratios it is possible to obtain equal values of ultimate load with lower values of ordinary reinforcement quantity. As shown in figure 45, for example, if a uniformly distributed ultimate load agent of 15 MPa is considered, a saving in reinforcement of almost 8 kg/m³ can be obtained, considering a value of $f_{Rk} = 2,7$

(20 kg/m³) or almost 3 kg/m³ with $f_{R3k}=5,5$ (40 kg/m³). In any case, respecting the requirements imposed by the standard (chapter 3.1), it is possible to obtain high values of uniformly distributed ultimate load agent.

In conclusion, the following study highlights the influence of the area ratio of reinforcement, so, in the optimization study, it's important to search the optimal ratio.

4.4 Redistribution of moments

This section is aimed to analyse how the moments are redistributed from their elastic value to the plastic one.

In statically indeterminate structures, moment distribution depends on the longitudinal variation in stiffness and this, in turn, on the stress-strain relationships of the materials. The most rigid sections tend to absorb more forces than the less rigid ones. So, when a section cracks, its stiffness declines, how it is shown in figure 50, and it takes smaller moments under increasing loads. This also occurs, but much more intensely, when a section becomes plastic since its stiffness becomes practically negligible and it is unable to receive any further increase in stress. [16]

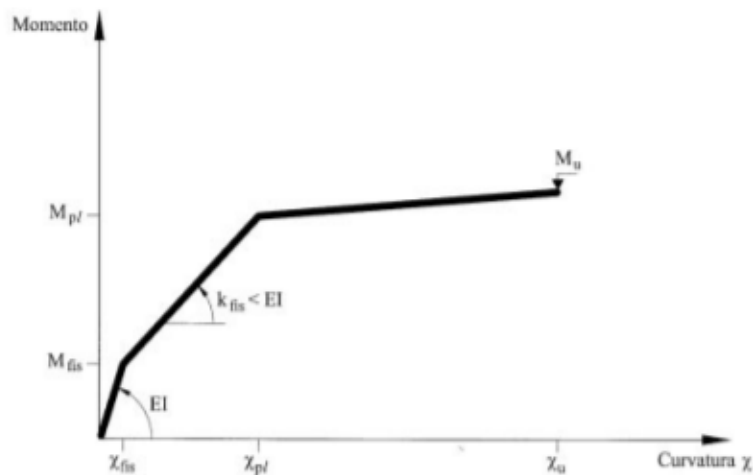


Figure 51: Simplified moment-curvature, $M-\chi$, diagram [16]

In the "Practical analysis of reinforced concrete structures with moment redistribution" it is clearly explained and illustrated how, in a qualitative way, the moments are distributed.

Bottom	Top	As,b [mm ² /m]	As,t [mm ² /m]	As,t/As,b [-]	ρ _{s,b} [%]	ρ _{s,t} [%]	CODE
Φ12/200	Φ12/200	565,5	565,5	1	2,82	2,82	2,82/2,82-1
Φ12/200	Φ16/200	565,5	1005,3	1,77	2,82	5,02	2,82/5,02-1,77
Φ12/200	Φ18/200	565,5	1276	2,25	2,82	6,38	2,82/6,38-2,25

Table 12: Cases studied

Through the use of Sap2000, once an ultimate distributed load equal a 15,2 MPa is established, the values of the elastic moment are obtained. In figures 52 and 53, it's shown the model deployed and the elastic moments obtained.

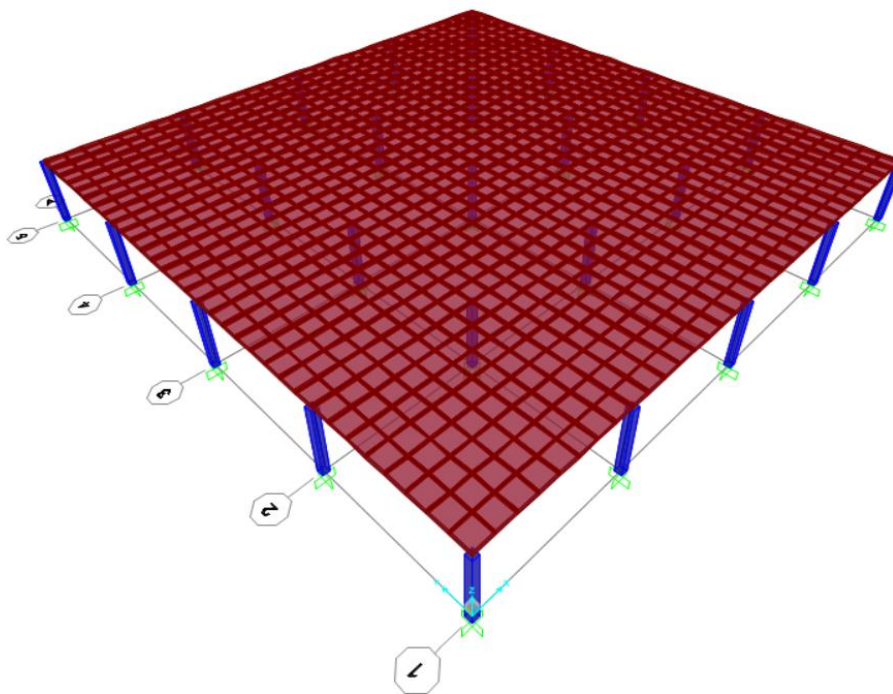


Figure 53: Flat slab model deployed using Sap2000

The mean value of the elastic moment is calculated along the support line of the central

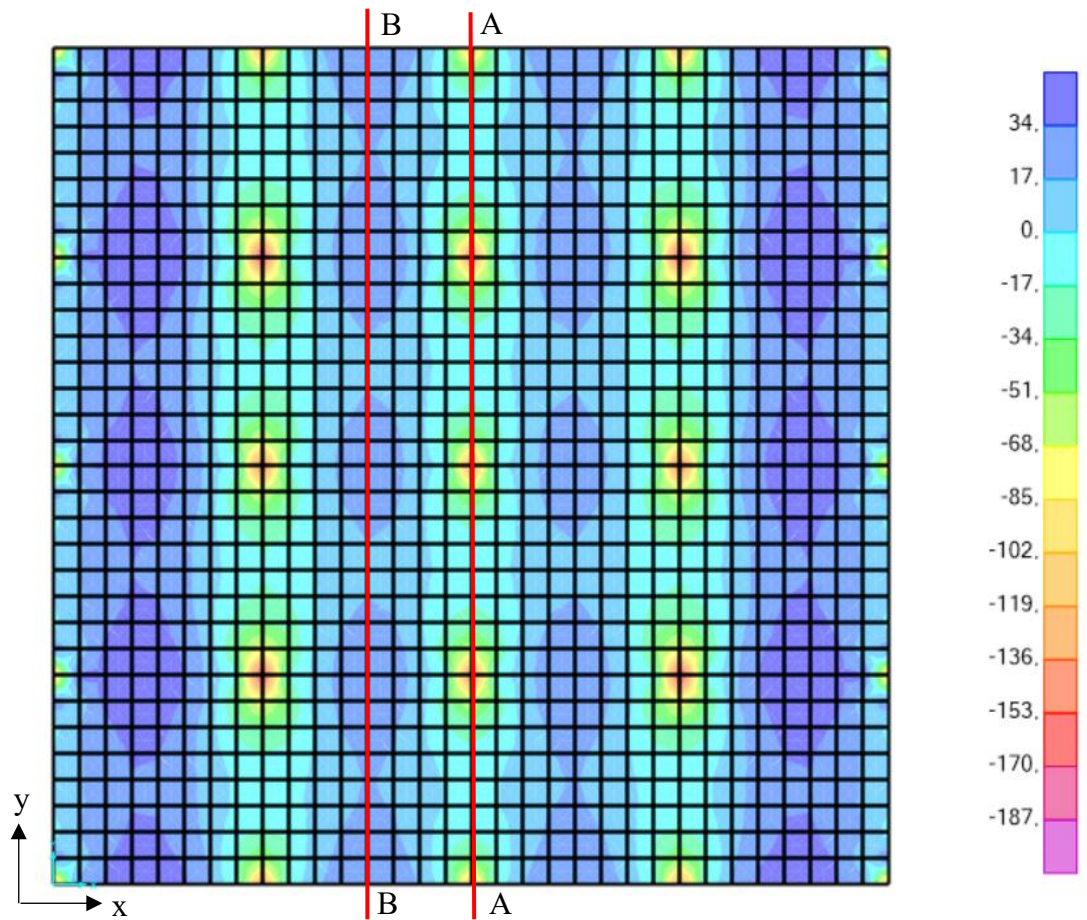


Figure 54: Elastic Moment along the y direction obtained from SAP 2000

pillars AA and along the center line of the internal panels BB. The following results are obtained:

- $M_{el,m}^+ = 24,3 \text{ MPa}$
- $M_{el,m}^+ = 40,3 \text{ MPa}$

Knowing the value of the mean elastic moment for a defined distributed ultimate load, it is possible to calculate by a linear equation, the value of the elastic moment for any load agent in the slab. Assuming the values of positive and negative reinforcements in table 12 and different values of f_r3k , it is possible to obtain the value of positive and negative ultimate moments. Given these values, the ultimate loads are obtained. So it's possible to calculate the mean elastic moment for any cases. Using equation 4.29, the percentage redistribution values of the moment are calculated.

$$\xi = \frac{(M_u - M_{el,m})}{M_{el,m}} \quad (4.29)$$

The following graph in figure 54 shows the results obtained.

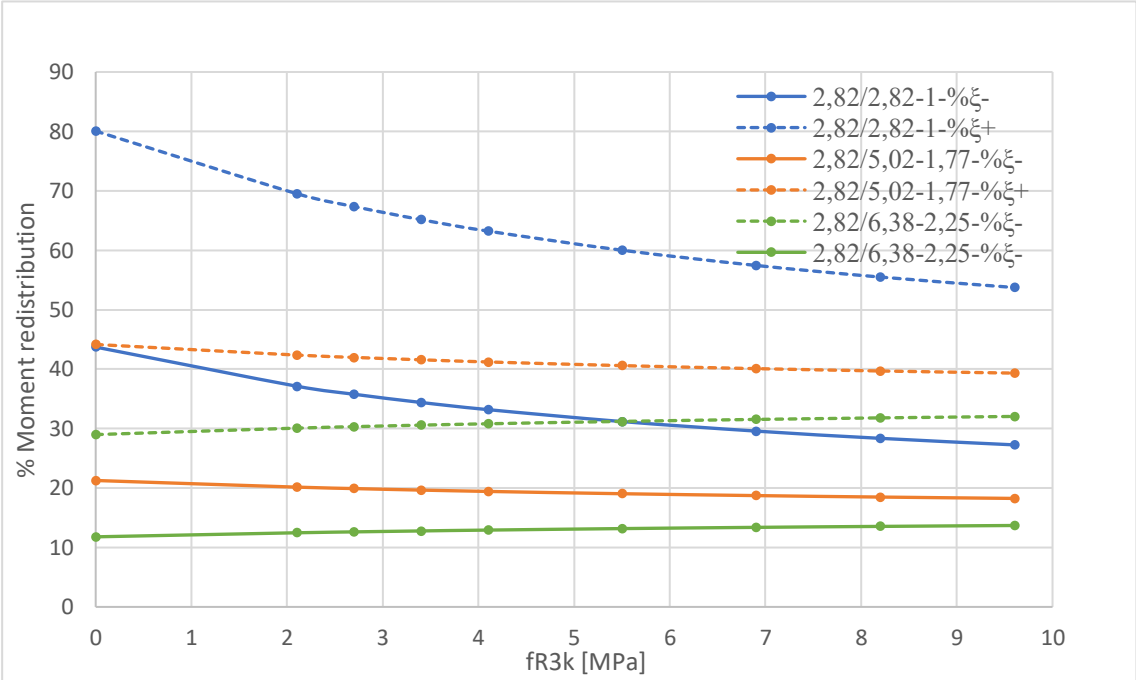


Figure 55: Percentual moment redistribution vs f_{R3k}

It is possible to observe from this graph that It's obtained elevated redistribution values when the ratio between the reinforcements areas is equal to 1. As the ratio increases, admissible redistribution values instead are achieved. It is also interesting how there is an asymptotic trend by increasing the value of the fibres.

In conclusion, it's important to check the values of the redistribution moments in order to guarantee structural ductility.

5 Optimization of Hybrid Flat Slab

As study of analysis, in order to find the optimal hybrid solution at ULS, the same model used for the parametric studies developed in chapter 4 has been considered. These are briefly summarized in the following table 13 and 14.

Geometry		Section		Materials			
				Concrete C50/60		Steel B500C	
n° span	4x4	b [mm]	1000	f _{ck} [MPa]	50	F _{yk} [MPa]	500
Length spans[m]	6x6	h [mm]	200	f _{ctm,fl} [Mpa]	5,7	F _{yd} [MPa]	434,7
Pillars [cm]	30x30	c [mm]	30	f _{cd}	33,3	Es [GPa]	210
				E _c [Gpa]	38,6	P [kg/m ³]	7850

Table 13: Flat slab proprieties

Fibre proprieties									
Fibre content [kg/m ³]	0	15	20	25	30	40	50	60	70
f _{R3k} [MPa]	0	2,1	2,7	3,4	4,1	5,5	6,9	8,2	9,6
f _{tu} [MPa]	0	0,466	0,6	0,75	0,91	1,22	1,533	1,82	2,13

Table 14: Fibre proprieties

After setting the design values, the ultimate agent load is calculated. As required by the EN 1992-1-1 [14], all the combinations of the design loads must be considered to obtain the most critical values of the internal actions. The design load results from the following combination:

$$E_d = \sum \gamma_G G_1 + \gamma_G G_2 + \sum_i \gamma_Q \psi Q_k$$

where G and Q represent permanent and variable actions respectively; the coefficients $\gamma_g = 1.35$, $\gamma_q = 1.5$ are the partial factors for actions; ψ is the factor for the combination of variable actions.

Assuming a value of thickness, which depends on span length through the equation, and the values of dead and live load, we obtained the following design loads.

Dead load		γG [KN/m ³]	h [m]	G [KN/m ²]	[KN/m ²]
Structural G1	Slab	24	0,2	4,8	4,8
Not structural G2	Pavement	20	0,02	0,4	2
	Mortar	20	0,02	0,4	
	Screed	18	0,04	0,72	
	Grout	20	0,02	0,4	
	Partition	1			
Live load Q					4
Ultimate load					15,2

Table 15: Values of dead and live loads

5.1 Static analysis

Once all the properties and the ultimate load have been defined, a calculation program deployed on MATLAB was used to calculate the minimum amount of reinforcement required to resist the defined load. Using the design approach present in chapter 3, the following figures and tables show the results obtained.

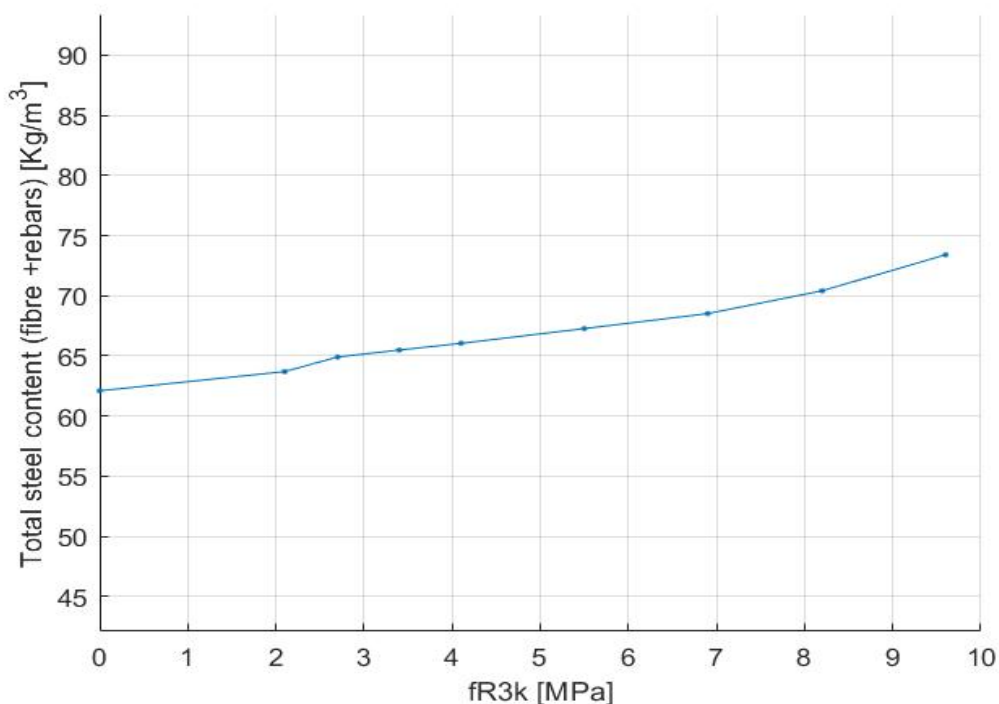


Figure 56: Total steel content vs. $fR3k$, for a flat slab containing the Hybrid Reinforcement designed according to the proposed design method.

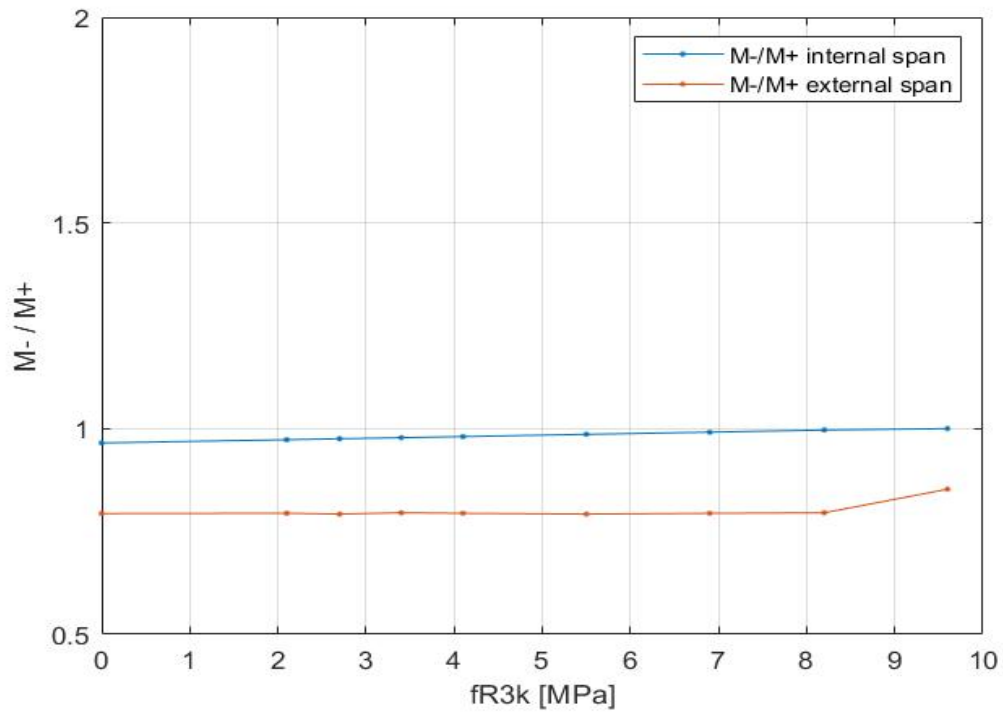


Figure 57: M-/M+ vs fR3k

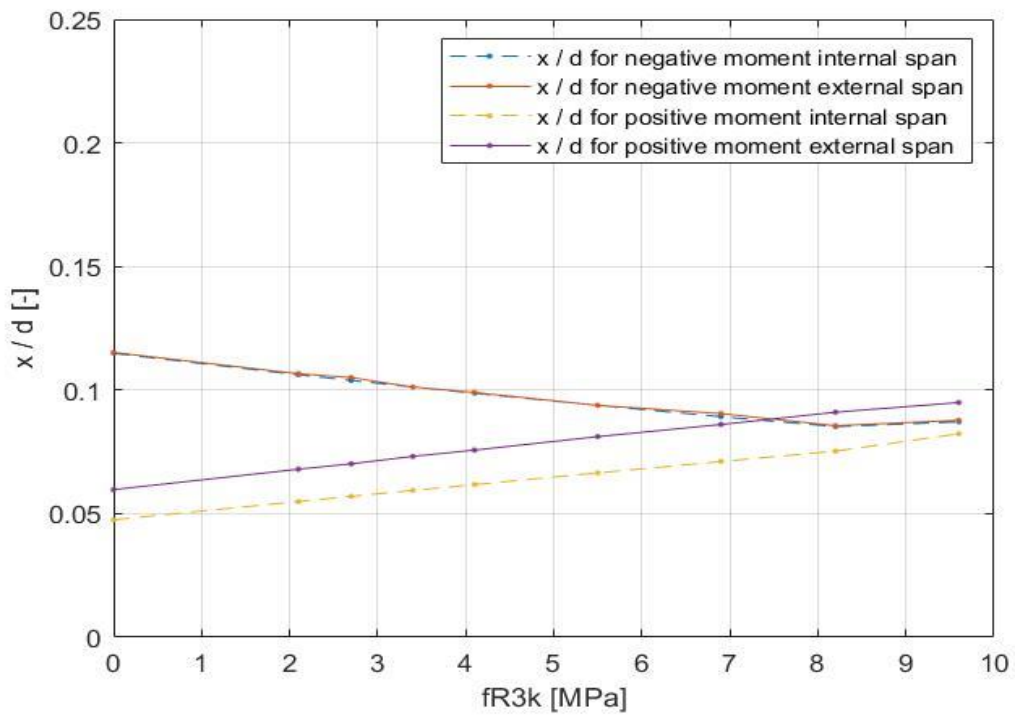


Figure 58: x/d vs fR3k

f _{R3k} [Mpa]	Internal spans		External spans		Total steel content		
	As,b [mm ² /m]	As,t [mm ² /m]	As,b [mm ² /m]	As,t [mm ² /m]	Fibre [kg/m ³]	Rebars [kg/m ³]	Total
0	524,7	1197	639,7	1210,3	0	62.5	62.5
2,1	402,2	912,1	522,2	925,6	15	49.1	64.1
2,7	367,4	831,5	492,4	831,5	20	45.3	65.3
3,4	326,7	738,0	451,7	741,6	25	40.9	65.9
4,1	286,2	645,0	411,2	658,2	30	36.4	66.4
5,5	205,2	460,7	335,2	465	40	27.6	67.6
6,9	124,5	278,5	259,5	278,2	50	18.9	68.9
8,2	49,8	111,0	184,8	125	60	10.8	70.8
9,6	0	0	95	17	70	3.8	73.8

Table 16: Results obtained for case analysed

From the results obtained, it can be deduced that the solution without reinforcement leads to the optimal solution value considering all the hypotheses defined in chapter 3. There is a slight increase in the total amount of steel when the fibre content increases. Table 16 shows that the theoretical areas of tops obtained are almost equal, so the final amount of reinforcement in the areas of the negative moment will be equal. While the values of bottom reinforcement in order to obtain an optimal solution have different values.

Considering the same design approach but using the results of elastic moment obtained on the file implemented on SAP2000, the curve f_{R3k} vs Total steel content has been calculated without searching the optimization value. The following moment are taken into account:

- Elastic positive moment in internal panels equal a 33MPa
- Elastic negative moment in internal panels equal a 160 MPa
- Elastic positive moment in external panels equal a 45MPa
- Elastic positive moment in external panels equal a 190 MPa

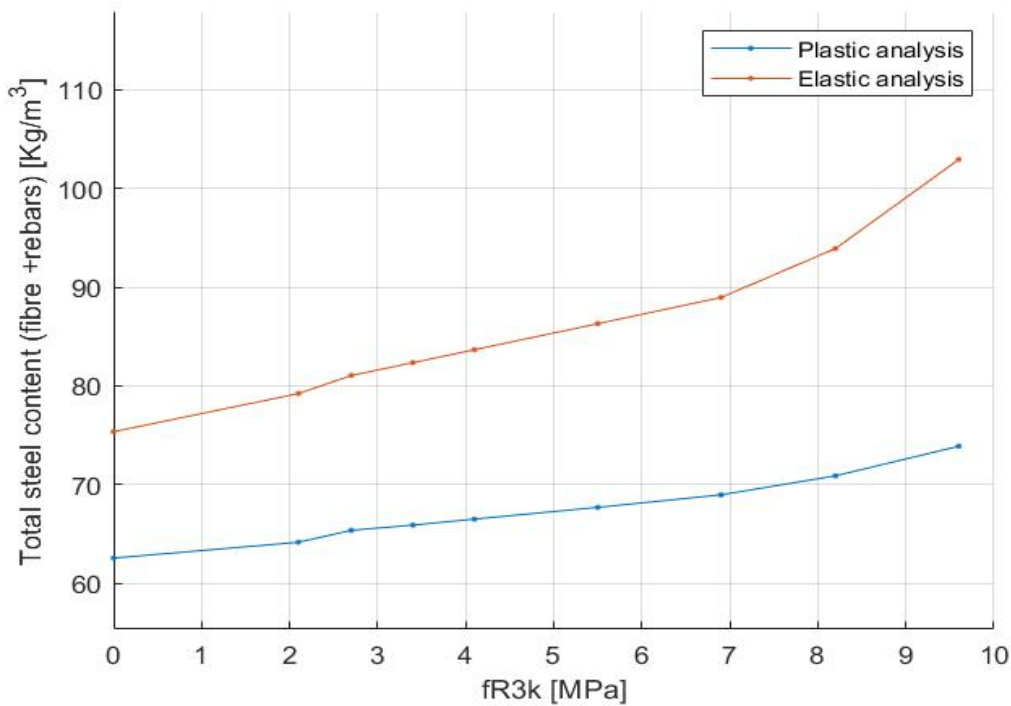


Figure 59: Total steel content vs. fR3k, for plastic and elastic analysis

From the results obtained it is evident that using the plastic theory and therefore the yield lines theory, it is possible to obtain an optimal solution compared to the one which would be obtained using the design moment values of the elastic moment. A reinforcement quantity of about 15 kg/m^3 can be saved.

Even if a minimum value is not reached adding the fibres, these nevertheless have a significant influence on the calculation of the ELS. Future studies, chapter 6, will be focused on checking the limits of ELS with these results obtained at USL. It is to be expected that for optimal values calculated at the ULS do not satisfy the limits imposed by the standards. So, it probably will lead to an increase in the amount of reinforcement for low fibres content values.

5.1.1 Verification at punching shear

Through the use of Sap2000, the reactions in the columns are calculated and the verifications to the punching shear are carried out by the equations contained in chapter 3.6.

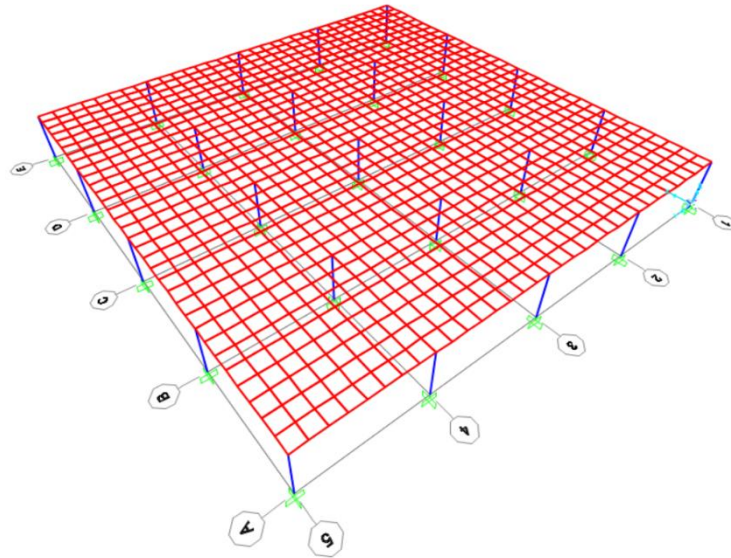


Figure 60: Flat slab model deployed using Sap2000

Given the symmetry of the slab, the punching verifications are carried out on the columns shown in table 17 and 18. Checks have been carried out for each quantity of fibre and all are being verified. The values for 2 different cases are shown below:

Column	F [kN]	F _{ed} [kN]	A _{s,t} [mm ² /m]	A _{s,b} [mm ² /m]	f _{R3k} [MPa]	V _{ed} [MPa]	V _{rc} [MPa]	V _{ed} < V _{rd}
A5	37	38,8	639	1210	0	0,22072	0,86133	V
A4	82	107	639	1210		0,34618	0,86133	V
A3	73	94,3	639	1210		0,3051	0,86133	V
B2	215	309	639	1210		0,57955	0,86133	V
B3	189	270	639	1210		0,50641	0,86133	V
C3	163	230	524	1197		0,43138	0,84098	V

Table 17: Verification at punching for f_{R3k}=0

Column	F [kN]	F _{ed} [kN]	A _{s,t} [mm ² /m]	A _{s,b} [mm ² /m]	f _{R3k} [MPa]	V _{ed} [MPa]	V _{rc} [MPa]	V _{ed} < V _{rd}
A5	37	38,8	411	658	30	0,22072	1,32495	V
A4	82	107	411	658		0,34618	1,32495	V
A3	73	94,3	411	658		0,3051	1,32495	V
B2	215	309	411	658		0,57955	1,32495	V
B3	189	270	411	658		0,50641	1,32495	V
C3	163	230	286	645		0,43138	1,29264	V

Table 18: Verification at punching for f_{R3k}=30

In any case, the stress values agents are lower than the shear strength of the concrete, this is due to the fact the high class of resistance of the concrete and the contribution of the fibres.

5.2 Parametric studies

Other different studies have been analysed changing some parameters keeping the previously set values, in order to verify which value can influence the optimization.

5.2.1 Influence of ultimate load

Other different studies have been analysed changing some parameters keeping the previously set values. First of all, it is changed the value of the live load. Using the Italian standards NTC, it's considered three different value of live load referred three different categories of construction use.

- $Q = 2$ [Mpa] $\rightarrow q_u = 12,2$, for residential and office areas
- $Q = 3$ [Mpa] $\rightarrow q_u = 13,7$, for areas susceptible to crowding, for example school and restaurant
- $Q = 4$ [Mpa] $\rightarrow q_u = 15,2$, for commercial areas

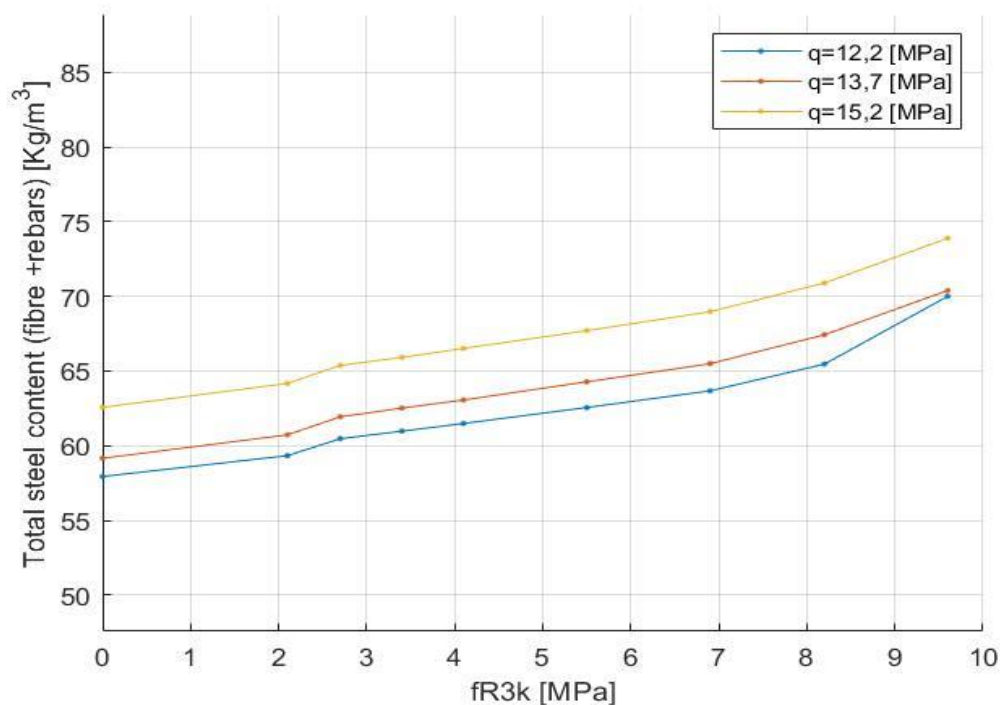


Figure 61: Total steel content vs. $fR3k$, for different ultimate loads

It is possible to notice that by increasing the distributed load, the total value of the reinforcement to be introduced obviously increases.

5.2.2 Influence of thickness of the flat slab

Then, it has changed the thickness of the flat slab, always keeping in mind the relation that limit the slab slenderness (t/L =thickness/span length) in the range:

$$\frac{1}{35} \leq \frac{t}{L} \leq \frac{1}{25}$$

Considering a length span equal a 6 m, the thickness has to be within these values

$$170 \leq t \leq 240$$

It has been considered three different value of thickness, for each thickness parameter, it's obtained the corresponding ultimate load, because of the dead load change.

- $h = 180 \text{ mm} \rightarrow q_u = 14,5 \text{ MPa}$
- $h = 200 \text{ mm} \rightarrow q_u = 15,2 \text{ MPa}$
- $h = 220 \text{ mm} \rightarrow q_u = 15,8 \text{ MPa}$

The results are shown in the following Figure 61.

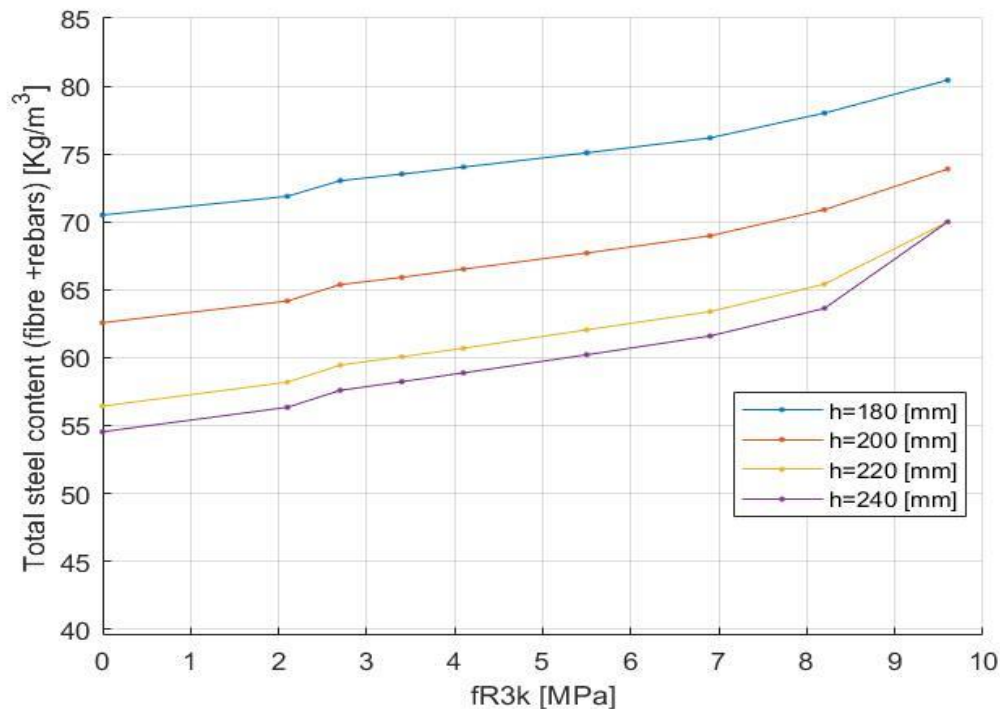


Figure 62: Total steel content vs. fR3k, for different thickness of the slab

This graph shows how the influence of the thickness of the slab affects the maximum amount of reinforcement. It is possible to observe a high saving of steel reinforcement. However, there are some disadvantages, as for example architectural or structural. If a building on several floors is considered, the loads acting on the pillars are gradually higher and can, therefore, lead to a different dimensioning of the pillars and foundations.

5.2.3 Influence of span number

Another study is carried out by changing the number of spans of a building. Three cases with three different span number cases are considered:

- 4x4
- 6x6
- 8x8

The below results are obtained in Figure 62

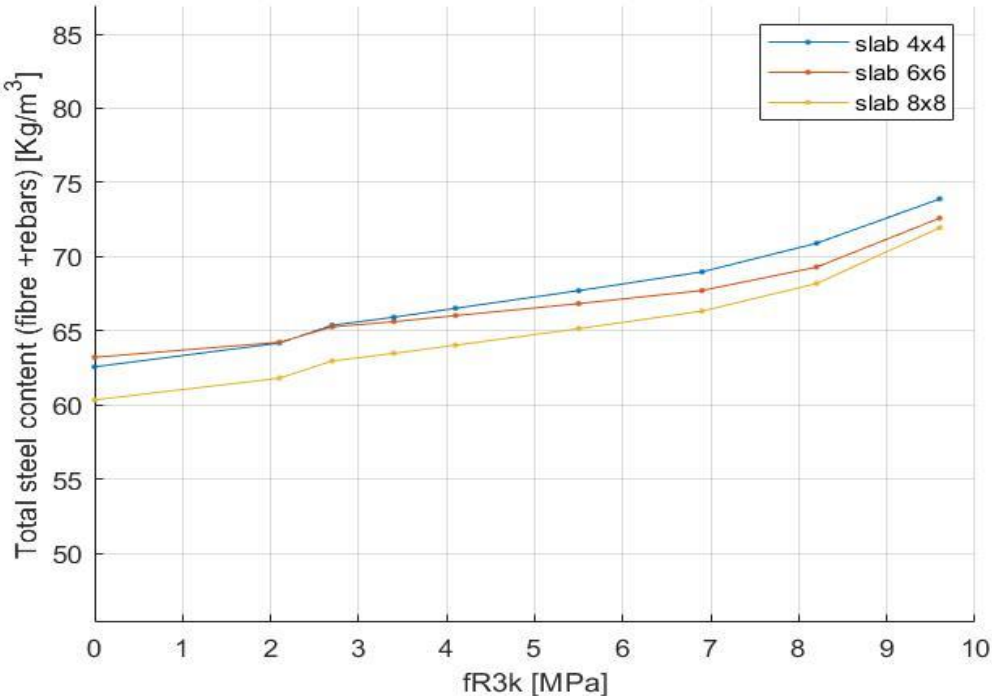


Figure 63: Total steel content vs. fR3k, for different span number

From the graph it can be observed that the optimization curve is lowered as the number of spans increases. This is due to the fact that the internal panels need a lower quality of reinforcement, therefore increasing the size of the floor, increase the number of internal panels and therefore a reduction in kg/m³ of steel content.

5.2.4 Influence of f_{R3m}

In addition, an interesting analysis has been performed, considering the average tensile strength value of the fibres and comparing it with the values obtained considering the characteristic values

$$f_{R3m} = \frac{f_{R3k}}{0.7}$$

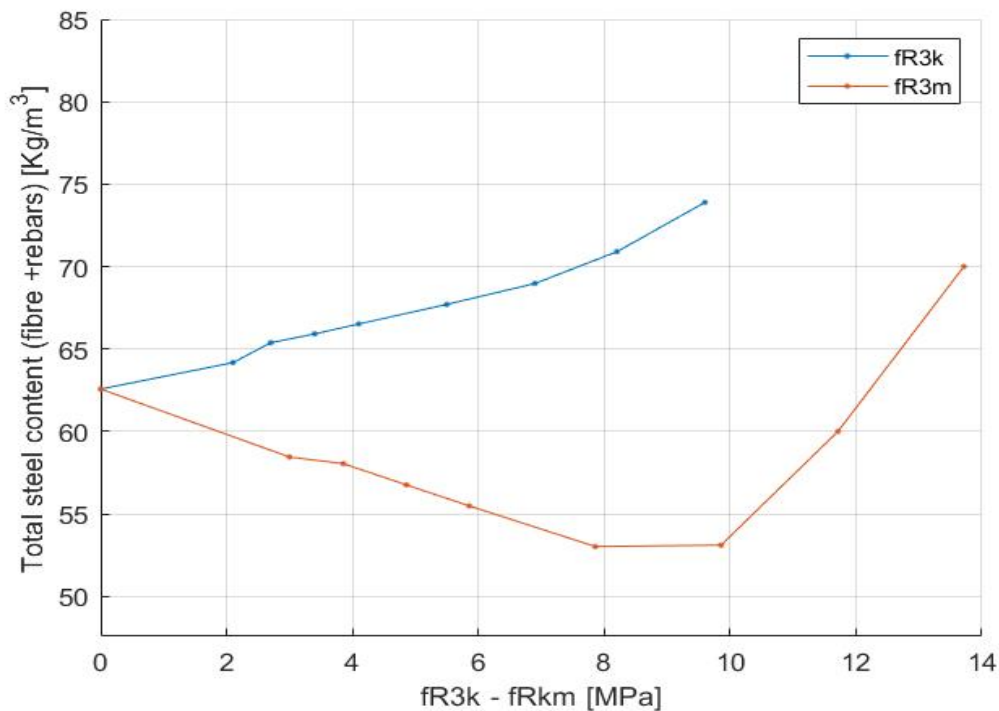


Figure 64: Total steel content for characteristic and mean tensile strength of fibre

As it can be deduced from this graph, it is possible to deduct that an increase in the resistant value of the fibres can lead to an optimization of the total steel content and rebars savings. So, this last analysis shows how the quality and property of the fibres is very important in the value of optimization. It is therefore very important to identify the best type of fibre to be used and carry out numerous laboratory tests to obtain a characteristic value mostly reliable and accurate.

5.3 Economic analysis

Another important aspect to consider is the economic aspect. In this work, only the cost of the materials and their installation have been taken into account. The average value of the standard €/kg of fibres is considered, which is € 1.5 with a certain deviation of 30%. As far as reinforcement is concerned, the values are obtained from the BEDEC - ITeC - Instituto de Tecnología de la Construcción [17], which takes into consideration the overall price of the reinforcement, i.e. in addition to the cost of the individual material, the price for the installation and the specialized employee have been taken into consideration. The final cost considered for the rebars is € 1.42/kg with a certain deviation of 10%. In the following figure, it's shown the oscillation costs obtained.

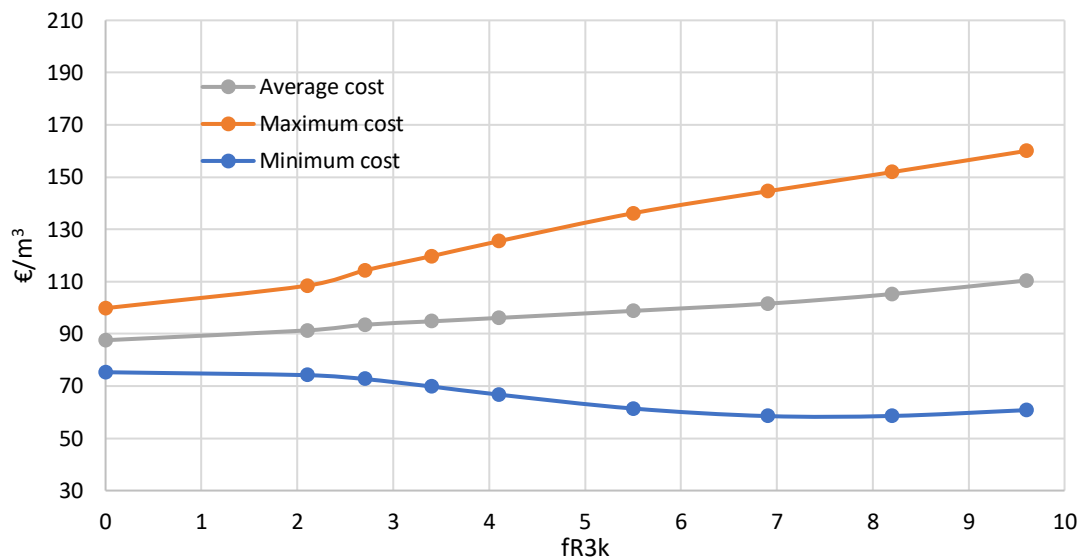


Figure 65. Oscillation costs [€/m³]

The following graph does not lead to an economic saving, obviously because the average cost of the fibres is higher than the cost of the reinforcement rebars.

But a key economic advantage is the reduction in construction time compared with the traditional installation of double layers of conventional reinforcing bars, stirrups, or other shear reinforcement. Time savings of several weeks for flat slab can be obtained; however, the economic costs and actual savings are based on a collection of individual gains obtained and measured using appropriate construction estimating tools and evidenced by the field data that support the decisions made to use this construction methodology.

Other important aspects in this brief analysis have not been taken into account. For example the SFRC can be directly pumped to elevated slabs, so the use of cranes for lifting reinforcing bars is eliminated. The overall simplification of the jobsite significantly improves the physical and labor-intensive tasks that would be otherwise needed if reinforcing bars were to be placed. This simplification has the potential to improve safety on the jobsite. A reduction in personnel for placing and finishing may also occur when compared with the traditional RC structures. There is also a saving in the volume of concrete, the SFRC may be somewhat thinner than the traditional slab when design verifications for serviceability and ultimate limit states are assessed. In conclusion, a total cost saving is obtained for a SFRC construction compared with traditional methods of reinforced concrete slab construction.

6 Conclusion

Fibre reinforcement extends the versatility of concrete as a construction material by overcoming the otherwise intrinsic brittleness and by improving the structural behaviour (crack propagation, flexural stiffness, ductility, ect), but also by the potential it has to simplify the construction process.

The results presented and discussed in this thesis yield the following conclusions:

- The proposed design method provides an easy and straightforward procedure for the designing of Hybrid Reinforcement flat slab at ULS by performing a plastic analysis of the structure.
- The fibres give an important contribution to the flexural behaviour of the structure and its presence in the concrete mix is able to provide the partial or even total substitution of the conventional reinforcement due to high residual tensile strength, ductility and toughness of the material.
- The results obtained show that using the theory of plastic for the design of a flat slab with the design approach considered, it is possible to have a saving on the total amount of reinforcement at ULS compared to the one that would be obtained with the values of elastic moment.
- This design approach considered do not lead to a minimum value for different fibre content. But by looking at the parametric studies, a minimum value is obtained if an average value of residual tensile strength is considered or if better fibres quality is used.

6.1 Future studies

Future studies will mainly aim to verify the optimization values at the serviceability limit state SLS, for any slab geometry and material properties. Once the best solution, that fulfil the ULS is found, it is necessary to verify the limits imposed from the standards at SLS and in particular the control-crack width. The technical standards impose values to be respected for the crack width, that is closely linked to the exposure class of the structural element, in order to ensure durability. Thanks several studies and analysis carried out, the role of the fibres in the crack width control is known. Therefore, the optimization curve could be modified in order to obtain all the standard requirements. Another interesting study is to find the best type of fibre able to obtain the best optimal solution in structural and economic terms.

References

- [1] S. M. F. Jensen and K. T. Jan Arve Øverli, “Numerical Investigation of a Post-tensioned Flat Slab with Steel Fibre Reinforcement,” *Dep. Struct. Eng*, 2013.
- [2] A. Abid and K. Franzen, “Design of Fibre Reinforced Concrete Beams and Slabs,” p. 128, 2011.
- [3] I. Löfgren, *Fibre-reinforced Concrete for Industrial Construction*. 2005.
- [4] A. C. I. Committee, *Report on Design and Construction of Steel Fiber-Reinforced Concrete Elevated Slabs*, no. 2. 2004.
- [5] K. ERICSSON, S.; FARAHANINIA, “Punching Shear in Reinforced Concrete Slabs Supported on Edge Steel Columns,” p. 148, 2010.
- [6] *Model code for Concrete Structures 2010*. 2013.
- [7] BS EN 14651, “Measuring the flexural tensile strength (limit of proportionality (LOP), residual),” *Br. Stand. Inst.*, vol. 3, pp. 1–17, 2005.
- [8] C. Ana Blanco Alvarez, Polit, Universitat Departament, “Characterization and modelling of SFRC elements,” March, 2013.
- [9] U. Gossla, “Development of SFRC Free Suspended Elevated Flat Slabs,” May, 2005.
- [10] X. Destrée and J. Mandl, “Steel fibre only reinforced concrete in free suspended elevated slabs: Case studies, design assisted by testing route, comparison to the latest SFRC standard documents,” *Tailor Made Concr. Struct.*, pp. 437–443, 2008.
- [11] C. Caprani, “Civil Engineering Design (1) Analysis and Design of Slabs,” 2006.
- [12] C. G. Gerard Kennedy, “Practical yield line design,” *Fiz. i Khimiya Obrab. Mater*, 2003.
- [13] fib, *fib Bulletin 57 - Shear and Punching Shear in RC and FRC Elements*, no. October. 2010.
- [14] “Eurocode 2: Design of concrete structures - Part 1-1 : General rules and rules for buildings,” no. 2, p. 227, 2004.
- [15] L. Facconi, G. Plizzari, and F. Minelli, “Elevated slabs made of hybrid reinforced concrete: Proposal of a new design approach in flexure,” *Struct. Concr.*, vol. 20, pp. 52–67, 2019.
- [16] A. R. M. B. Andrés Doñate Megías, José Calavera Ruiz, “Practical analysis of reinforced concrete structures with moment redistribution,” p. 89.
- [17] <https://itec.es/servicios/bedec/> BEDEC - ITeC - Instituto de Tecnología de la Construcción

Acknowledgements

I would first like to thank Prof. Albert de La Fuente for all the time he dedicated to me and for all the endless advice he gave me during the whole realization of this document. I will always remember his kindness, humanity, reassurance and humor which accompanied the crucial moments of my work.

I must express my gratitude to Stanislav Aidarov (PhD), whose role in this document has been fundamental. I will never forget his limitless patience and passion for supervising me. His valuable knowledge was kindly made available to me in the crucial points of the thesis.

I am grateful to Prof. Maurizio Taliano for having given me the opportunity to take this exciting path abroad.

I will always carry in my heart all the people I met during my experience in Barcelona, all the friends I made, who have made me fall in love with this beautiful city and country. It thanks to them that I grew up and I opened my mind.

My thanks also go to my lifetime friends. I have always appreciated their deep affection.

Finally, I want to thank the most important persons, my parents and my brother, for the trust and love they give me. They have always supported me in these years in every choice I made and I am sure they will still support me in every single step I will make in the future. I want to say to them a big "vi voglio bene".